VOLUME 29 DECEMBER 1951 NUMBER 12

Canadian Journal of Technology

Editor: G. A. LEDINGHAM

Published by THE NATIONAL RESEARCH COUNCIL
OTTAWA CANADA

CANADIAN JOURNAL OF TECHNOLOGY

This was formerly *Section F, Canadian Journal of Research*. The change to the new name took place January 1, 1951. The CANADIAN JOURNAL OF TECHNOLOGY is published twelve times annually.

The CANADIAN JOURNAL OF TECHNOLOGY is published by the National Research Council of Canada under the authority of the Chairman of the Committee of the Privy Council on Scientific and Industrial Research. Matters of general policy are the responsibility of a joint Editorial Board consisting of members of the National Research Council of Canada and the Royal Society of Canada.

The CANADIAN JOURNAL OF TECHNOLOGY and the CANADIAN JOURNAL OF CHEMISTRY have been chosen by the Chemical Institute of Canada as its medium of publication for scientific papers.

The National Research Council of Canada publishes also the following Journals: *Canadian Journal of Botany, Canadian Journal of Chemistry, Canadian Journal of Medical Sciences, Canadian Journal of Physics, Canadian Journal of Zoology.*

EDITORIAL BOARD

Subscription rate: $3.00 a year. All enquiries concerning subscriptions should be addressed to the CANADIAN JOURNAL OF TECHNOLOGY, National Research Council, Ottawa, Canada. Special rates can be obtained for subscriptions to more than one of the Journals published by the National Research Council.

Canadian Journal of Technology

Issued by THE NATIONAL RESEARCH COUNCIL OF CANADA

VOL. 29 DECEMBER, 1951 NUMBER 12

KINETICS OF THE THERMAL DECOMPOSITION OF WOOD[1]

BY R. H. WRIGHT[2] AND A. M. HAYWARD[3]

Abstract

The rate of decomposition of dry western red cedar and western hemlock when introduced suddenly into an atmosphere of nitrogen at 500°, 700°, and 900°C. has been studied. For cubical pieces the reaction is approximately of the one-half order; for disks it is of zero order. For cubes the rate constant is directly proportional to the specific surface and to the temperature, and the proportionality constants are the same for both species of wood.

Introduction

This paper describes a study of the effect of particle size and of temperature on the rate of decomposition of western red cedar and western hemlock. The experiments were part of a study of methods of producing fuel gas from waste wood.

In the usual commercial processes of wood distillation, where a retort is filled, closed, and heated externally, a long time is needed to bring the large mass of wood up to the final temperature. These experiments were designed to find out what happens when small pieces of wood are suddenly introduced into an inert atmosphere at high temperature.

Experimental Method

The reaction vessel was a Hevi-Duty retort furnace of about 60 liters capacity made of stainless steel and heated externally by resistance elements. The temperature was regulated automatically by a Foxboro Potentiometer Pyrometer and a Foxboro Potentiometer Controller.

The heat resistant steel lid of the retort was sealed in place with a mixture of zirconite and Hyflo Supercel moistened with sodium silicate and set by heating after the lid was clamped in place. The underside of the lid was insulated by a thin steel plate supporting a disk of Johns Manville Superex Insulation 3 in. thick.

[1] *Manuscript received June 19, 1951.*
Contribution from the Division of Chemistry, British Columbia Research Council, Vancouver, B.C.
[2] *Head, Division of Chemistry, B.C.R.C.*
[3] *Junior Chemist, B.C.R.C.*

The wood specimens were dropped into the retort by inverting a small steel bucket set near the top of a 2 in. pipe which passed through the center of the cover and was closed by a screw cap.

To provide an inert atmosphere the retort was thoroughly flushed with nitrogen from a cylinder before each experiment.

The decomposition of the wood was followed by measuring the increase in pressure due to the gas liberated. A diaphragm manometer was constructed by cementing a S.R.-4 strain gauge to the center of the surface of a steel diaphragm. Deflection of the diaphragm under pressure altered the resistance of the strain gauge and produced a deflection of the pen of a Brush Oscillograph. This gave a trace like that shown in Fig. 1. Since the frequency response of the

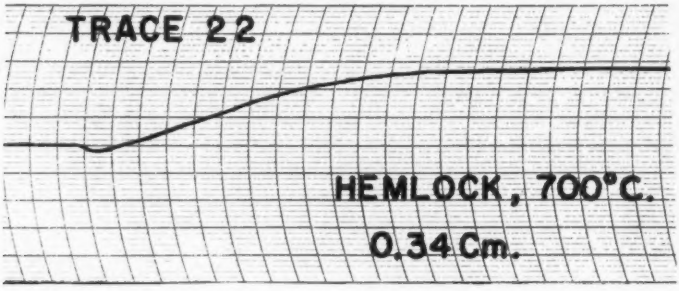

FIG. 1.

Brush Oscillograph extends to 100 c.p.s., the response of the recording system was effectively instantaneous. A calibration curve was made by comparing the readings directly with those of a mercury manometer.

The wood used was western red cedar and western hemlock. It was cut into cubes ranging from 19 mm. to 3 mm. edge. The weights of the samples varied between 1.5 gm. and 3.3 gm. With the larger cubes only one or two were used while as many as 140 of the smaller blocks were dropped at one time. The specimens were dried in an oven at 105°C. for at least 24 hr. before being used. A few tests were made with circular disks cut parallel and at right angles to the grain of the wood.

Treatment of the Results

The traces drawn by the Brush Recorder were treated as follows:—

The deflections corresponding to various times were read to 0.1 mm. using a lens. The corresponding pressures were then read off from the calibration curve and tabulated. Each tabulated value of the pressure was then expressed as a percentage of the final pressure, ie., 100 P/P_∞. Values of 100 $(1 - P/P_\infty)$ were computed. These values corresponded to the percentage of the original wood still undecomposed at any instant.

By trial, it was found that plots of $(100(1 - P/P_\infty))^{\frac{1}{2}}$ vs. time, t, were substantially straight lines as shown in Fig. 2.

This indicates that for cubes the reaction is kinetically of the order $\frac{1}{2}$. Thus, if

$$100\frac{dP/P_\infty}{dt} = k(100(1 - P/P_\infty))^{\frac{1}{2}}$$

then, on integrating

$$(100(1 - P/P_\infty))^{\frac{1}{2}} = -\frac{k}{2}t + \text{const.}$$

which has the form of a straight line whose slope is $-k/2$, when $(100(1 - P/P_\infty))^{\frac{1}{2}}$ is plotted against t.

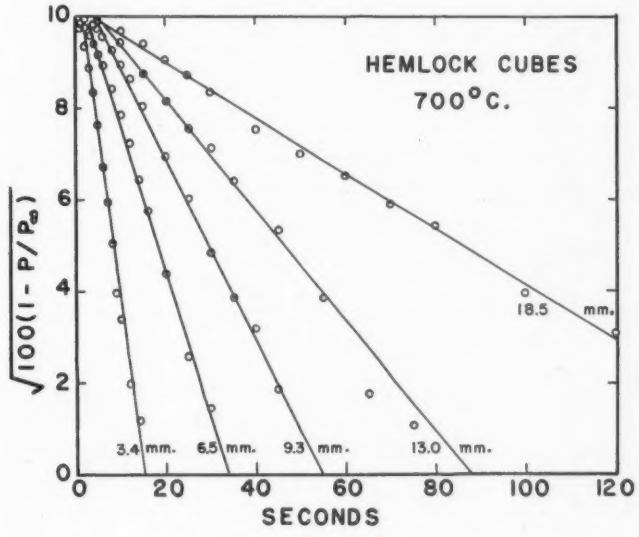

FIG. 2.

The data from each trace were plotted as shown in Fig. 2 and straight lines were drawn through the points. The slopes of these lines were determined and tabulated.

Usually, the straight line relation was not established until the reaction had been proceeding for a short time. Owing to the crowding of the points, this initial retardation of the reaction does not show well in Fig. 2 but is discussed more fully below. In the experiments at 500°C. the reactions were slow and the straight line relationship was not always as clear-cut as at the higher temperatures.

The variation of the rate constant k with the size of the cubes was then studied. Taking the length of the cube edge as L it was found that k varied

inversely with L. The graphs for cedar and hemlock at corresponding temperatures showed a difference in slope, which turned out to be due to the difference in density.

Thus, when k is plotted against $1/L$, in effect it is being plotted against the area per unit volume of wood. In order to plot k against the area per unit weight of wood, i.e. the specific surface, the abscissa must be $1/LD$, where D is the density of the material. The average density of oven-dry western red cedar is about 0.34 and western hemlock as about 0.43.

When the various values of k for cedar and hemlock were plotted against $1/LD$, a single set of curves covering both species of wood was obtained, as shown in Fig. 3. The various straight lines appear to cut the X axis at the same point, approximately where $1/LD$ equals 0.75.

Hence, a single set of equations can be set up of the form:

$$1/LD = ak + b$$

where $b = 0.75$

$$a = d(1/LD)/dk.$$

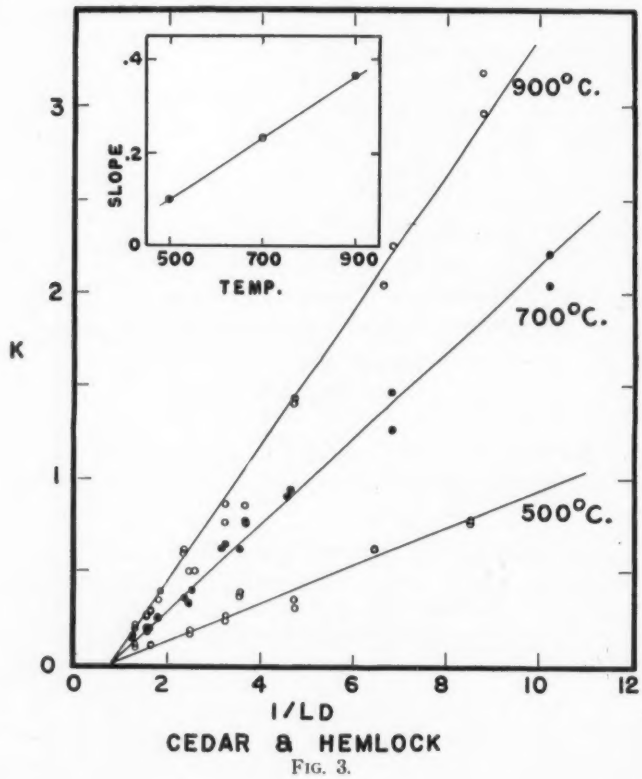

CEDAR & HEMLOCK

FIG. 3.

By plotting $1/a(= dk/d(1/LD))$ against T, a straight line is obtained as shown in the inset to Fig. 3. In constructing this figure a certain amount of latitude is possible in placing the straight lines. The positions chosen correspond to the constants given in the following equation:—

$$1/a = 0.00065\,T - 0.4$$

where T is the absolute temperature in °K.

This may be combined with the preceding equation to give:

$$k = (1/LD - 0.75)(0.00065T - 0.4) \quad (1)$$

where k = the rate constant
L = the cube length in cm.
D = the wood density in gm./cc.
T = the absolute temperature in °K.

and this equation applies to both cedar and hemlock.

From the equation $(100(1 - P/P_\infty))^{\frac{1}{3}} = -\frac{1}{2}Kt + \text{constant}$, when $t = 0$, $P = 0$ and the constant $= 10$. Therefore:—

$$\tfrac{1}{2}kt = 10(1 - (1 - P/P_\infty)^{\frac{1}{3}}).$$

If t_{99} is the time required for 99% of the wood to decompose,

then $\tfrac{1}{2}kt_{99} = 10(1 - (1 - 0.99)^{\frac{1}{3}})$
$= 9$
and $t_{99} = 18/k.$ (2)

This equation in conjunction with the Equation (1) enables the decomposition time for wood cubes of any size to be calculated at any temperature covered by the data. For example, we may take the case of hemlock cubes of 0.34 cm. edge at 700°C. From Equation (1), $k = 1.41$ and from Equation (2) $t_{99} = 12.8$ sec. Fig. 1 shows an experimental trace obtained for the decomposition of hemlock cubes of this size at 700°C. In Fig. 4, pressures corres-

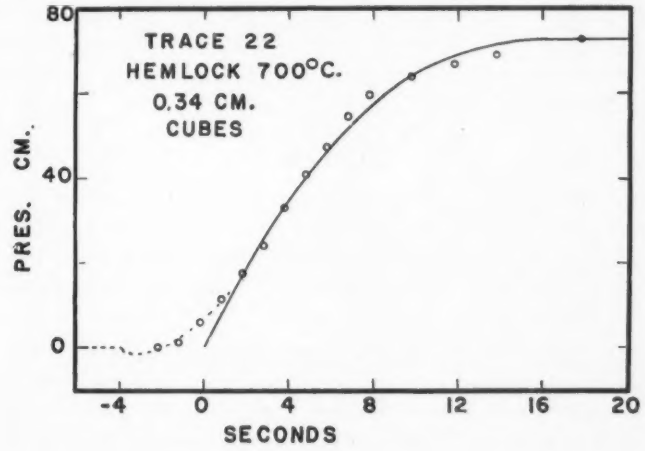

FIG. 4.

ponding to a number of points on the trace are plotted. The solid line shows the decomposition rate calculated from the value $k = 1.41$. The experimental points were plotted with a shift in the time axis so as to coincide with the calculated curve at the middle of the pressure rise.

As can be seen, the agreement is fairly good except at the beginning of the decomposition where there is a brief drop in pressure lasting about 1.5 sec. Following this drop a period of about 2 sec. was required for the reaction to work up speed.

It seems likely that the initial retardation is due to cooling of the gas in the retort and is inseparable from any process in which cold wood is suddenly introduced into an environment of hot gas. However, the magnitude of the retardation would depend on the circumstances of the particular process, for example, the stirring of the gas and the initial temperature of the wood. From an examination of Fig. 4 the retardation appears to be $15 - 20\%$ of the total reaction time.

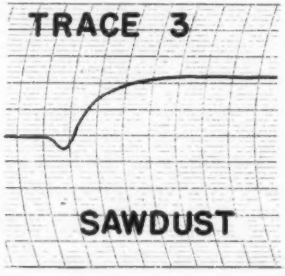

FIG. 5.

Fig. 5 shows the trace obtained when a sample of sawdust was decomposed. The initial retardation was slightly less than 1 sec. and the total reaction time was about 5 sec., so that the correction for the initial retardation estimated above appears to be fairly satisfactory.

Discussion

Since the high temperature, primary decomposition of wood is exothermic, the reaction should proceed at a rate largely independent of the rate at which heat penetrates into the specimen from outside. Furthermore, in view of the porosity of charcoal, the gaseous products of the decomposition should escape readily.

The rate of the decomposition reaction itself and the rate at which it is propagated through the wood are closely connected, but are probably independent to the extent that the rate of propagation depends largely on the speed with which heat from the zone of active decomposition can penetrate forward to the next layer of undecomposed wood.

If wood were perfectly isotropic and if the rate of decomposition were determined by the rate of propagation of the reaction, the decomposition could be regarded as taking place in a thin zone which travelled inwards from the surface. The area of this zone at any instant would be proportional to the 2/3 power of the amount of wood still undecomposed at that instant. Thus, the reaction would kinetically be of the 2/3 order.

If, however, wood were extremely anisotropic so that the reaction was propagated at a very much faster rate parallel to one axis (e.g. along the grain), then the area of the reaction zone would remain constant as it advanced through a rectangular piece and the reaction would be of zero order.

It seems probable that the actual situation is intermediate between these two extremes which would account for the observed rate being approximately of order 1/2.

In order to test this hypothesis, a few experiments were made at 600°C. using disks of cedar and hemlock approximately 2 cm. in diameter and 0.3 cm. thick. Fig. 6 shows the results for cedar. The decomposition rate for disks cut across the grain is approximately twice that for disks cut along the grain. The plot of $(100(1 - P/P_\infty))$ vs. time is more nearly linear than those of the same function to the power $\frac{1}{2}$, showing that the decomposition of disks is approximately of zero order kinetically. This is to be expected for thin pieces presenting a large flat surface. Moreover, as can be seen from the figure, the decomposition of disks cut across the grain is more nearly a zero order process than that of disks cut parallel to the grain, confirming the faster reaction in the direction of the grain.

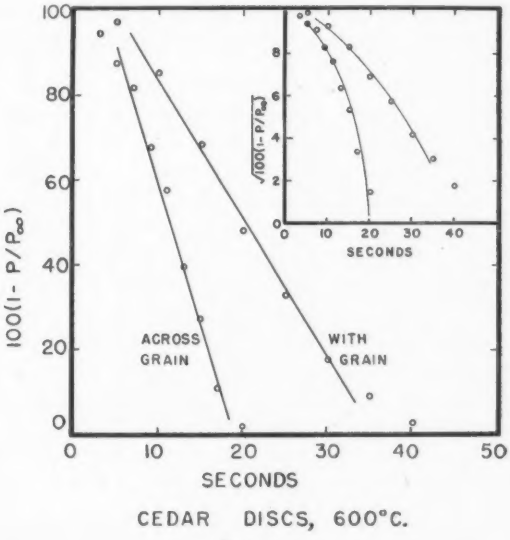

FIG. 6.

It may therefore be concluded that the reaction takes place in a zone or shell which advances inward from the surface, the rate of advance is higher along the grain than it is across the grain. The effect of particle size is to alter the specific surface of the wood and hence the area of the reaction zone. For a given specific surface the reaction rate is substantially the same for both cedar and hemlock. This suggests that the factor which controls the over-all rate of the decomposition reaction is not the detailed chemical composition of the wood but rather, a physical factor.

The most probable controlling factor is the rate at which heat from the reaction zone is passed forward to the undecomposed wood. This is strongly supported by the fact that the rate constant is directly proportional to the temperature.

If we have a hot reaction zone at a temperature T_R bounded on one side by cold wood at a temperature T_w and on the other side by hot gas at a temperture T_g, then the heat developed in the reaction zone will be lost, partly to the wood on one side and partly to the gas on the other side. If Q is the heat generated in the unit area of the reaction zone we can write:

$$Q = A(T_R - T_w) + B(T_R - T_g)$$

where A and B are transfer coefficients. On rearranging,

$$\begin{aligned} A(T_R - T_w) &= Q - B(T_R - T_g) \\ &= \text{constant} + BT_g. \end{aligned}$$

If the rate of advance of the reaction zone depends on the rate at which undecomposed wood can be brought up to the decomposition temperature, the effect of the gas temperature on the reaction rate would be governed by the above equation which is precisely of the form found by experiment.

THE OXIDATION OF CARBON MONOXIDE BY SOLID SILVER PERMANGANATE REAGENTS

III. EFFECT OF METHOD OF PREPARATION ON ACTIVITY[1]

By G. A. Grant, Morris Katz, and R. Riberdy

Abstract

The optimum conditions for the production of the most active silver permanganate reagent granules of desirable hardness have been derived. Precipitation of silver permanganate on powdered zinc oxide carrier, pressing the wet product in a mold at 10 tons per sq. in., and curing the molded cakes for 28 days at room temperature produced granules of suitable hardness and maximum activity.

Introduction

It has become evident from laboratory and pilot plant preparations of the silver permanganate – zinc oxide reagent that several steps in the preparation greatly influence the efficiency and life of the finished product. Other investigators working with other catalysts have reported on the effects of curing and aging and also the effect of molding pressure in compounding the materials (1, pp. 267-289). This report describes the results of a study of methods of mixing the ingredients, aging, curing, and the influence of pressure on the activity and hardness of the granules.

Methods

General Method of Preparation

A potassium permanganate solution (246 gm. per 3 liters) was prepared by dissolving the salt in water at 60°C., stirring, and cooling to 30°C. A thick creamy paste was made by mixing zinc oxide (255 gm.) and a silver nitrate solution (240 gm. per 150 ml.). The potassium permanganate solution was added to the zinc oxide – silver nitrate paste and the mixture stirred vigorously for one hour at room temperature. The reaction mixture was cooled to 0°C. and held at this temperature for at least two hours. The product was filtered in a Buchner funnel, employing a fine flannelette cloth as a filter pad. When the filtration was complete, the filter cake was packed with a flat-end glass rod or spatula until all the excess mother liquor was freed from the solid. The product was washed three times with small portions of cold distilled water. The filter cake was removed and transferred to a mold and pressed at 3 to 10 tons per sq. in. This removed the final traces of the mother liquor and packed the soft muddy residue into a solid bricklike cake. The material was stored in a dark room for 3 to 28 days to allow the product to cure. After curing, it was

[1] *Manuscript received August 13, 1951.*
Contribution from Defence Research Chemical Laboratories, Ottawa, Canada. Issued as Report No. 71.

broken up into small granules, usually, to screen size of −8+24 mesh Tyler. The granules, in some cases, were given an additional aging period of 72 hr. at 60°C.

Activity Tests

A 4 cm. column length of reagent was placed in a glass tube with a diameter of 2.82 cm. One per cent carbon monoxide in air mixtures at a relative humidity of 85-95% was passed through the column at a linear velocity of 625 cm. per min. The reaction tube was placed in a water bath at 30°C. These conditions were employed for all tests, unless otherwise specified. The purification of the carbon monoxide, the apparatus employed for the testing, and the method of analyzing for escaping carbon monoxide concentration has been previously reported (2, 4, 6). The breakdown time of the material was taken as the time when 0.03 or 0.1% carbon monoxide was escaping from the column. The column was then operating at 90-97% efficiency.

Hardness Test

The sieve hardness test employed was similar to that specified for the American Hardness Test, the difference being that five steel balls, 3/8 in. in diameter, and five balls, 1/2 in. in diameter were used and that the material was shaken on the Ro-tap machine for 15 min.

Experimental

The Effect of Methods of Mixing on Breakdown Time

As little was known about the preparation of this type of reagent, it was thought advisable to explore the methods of depositing the silver permanganate on the zinc oxide, and also the effect of adding ground reagent to the mixture, to employ some of the waste material from the screenings.

Preparation 1: (31 mole %, silver permanganate, 69 mole %, zinc oxide) was prepared as previously outlined, except that the zinc oxide was added to the potassium permanganate solution. The mixture was stirred and the silver nitrate solution added.

Preparation 2 was the same as previously outlined in the general preparation section, except that 33 % of fines from screenings were added to the mixture.

Preparation 3: Dry silver permanganate and zinc oxide powder were mixed dry and then just enough water added to form a very thick slurry mixture, to enable the material to be placed in the mold.

Preparation 4 was the same as that described in the general preparation and was employed as a control sample. These preparations were all aged for 28 days and activity measurements made. Results are given in Table I. It is evident that preparation of the reagent by first making a paste of the zinc oxide – silver nitrate solution and then adding the potassium permanganate solution produced the reagent with the longest breakdown time. It is evident,

TABLE I

EFFECT OF METHODS OF PREPARATION ON BREAKDOWN TIME

Preparation No.	Method	Breakdown time, min. 90% efficiency
1	Zinc oxide added to $KMnO_4$ solution, followed by $AgNO_3$ solution	87.5
2	Fines incorporated in standard batch	81.0
3	Mechanical mixture of $AgMnO_4$ and ZnO	73.0*
4	Standard method	95.25

* *When aged for 148 hr. at 60°C., B.T. decreased to 29 min.*

also, from Table I, that fines from previous preparations may be added to a new batch without a great loss in activity.

The effect of aging at room temperature of a mechanical mixture and the silver permanganate – zinc oxide prepared as described in Preparation 3, is shown in Fig. 1. It is evident that the silver permanganate in the reagent prepared by simple mechanical mixing decomposed at a faster rate than the control sample.

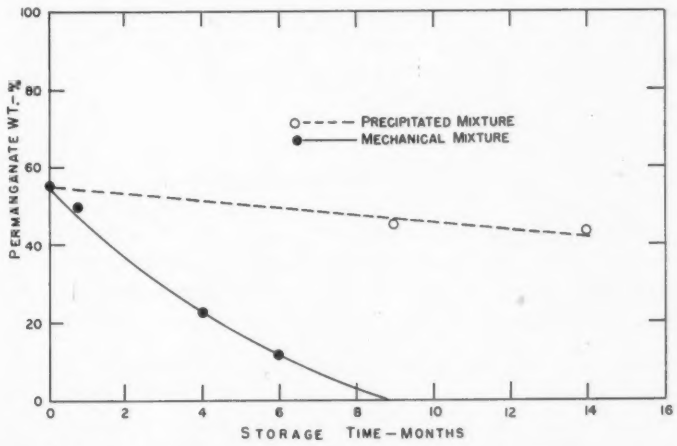

FIG. 1. *Effect of method of preparation of silver permanganate – zinc oxide reagent on stability.*

Effect of Molding Pressure and Curing Time

The effect of molding pressure and curing time on breakdown time was investigated. Molding pressures from 3 to 10 tons per sq. in., and curing times from 3 to 28 days were employed. The results are given in Table II. It is evident from Table II that an increase in both molding pressure and curing time results in an increase in breakdown time. When the pressure was increased from 4 tons to 10 tons per sq. in., the material showed an improvement in breakdown time from 55 to 67 min. for the reagent cured for three days, and an improvement

TABLE II

EFFECT OF PRESSING PRESSURE AND CURING TIME ON BREAKDOWN TIME

Pressure, tons/sq. in.	Curing time, days	Breakdown time, min. (97% efficiency)
3	14	34
	28	45
4	3	55
	14	70
	28	72
5	3	56
	14	64
	28	73
7.5	3	64
	7	71
	14	94
	28	103
10	3	67
	14	71
	28	104

in breakdown time from 72 min. to 104 min. for the material cured for 28 days. The increase in curing time from 3 days to 28 days resulted in an increase in breakdown time at all molding pressures. This was more pronounced at the higher pressures of $7\frac{1}{2}$ to 10 tons per sq. in. The best reagent was prepared by employing a pressure of 10 tons per sq. in., and a curing time of 28 days. This reagent gave a life of 104 min.

The Effect of Grinding on the Yield of Granules

In breaking the aged cake to the desired granule size (usually $-8+24$ mesh Tyler) there is considerable loss of material due to powdering either in the initial stage of breaking or in the screening operation on the Ro-tap machine. In early experiments, yield of granules amounted to 35 to 40%. Since this was considered an unsatisfactory feature in production of the reagent, a number of methods of crushing and screening were tried.

In preliminary trials, various combinations of breaking to different sizes with a hammer and various types of screening in the Ro-tap machine were tried, but best yields were obtained when the material was broken into very fine pieces before screening. The yields varied from 44.5% to 63.9%, depending on initial crushing to pieces from approximately 1/2 in. to 1/16 in.

In a large scale operation, a machine to replace the preliminary hand-breaking one is desirable. A hammer mill and ball mill were tried first but they reduced the cake to a fine powder rather than to lumps or granules. Finally, by employing, for the preliminary breaking, a combination of a Denver jaw crusher, 5×6, and a coffee mill, and then screening in a Ro-tap machine, satisfactory results were obtained. The jaw crusher was set at its finest setting and the coffee mill set at medium grind.

A pilot plant trial, involving 103 lb. of reagent, was carried out. The reagent was prepared in 47 small batches, each batch being crushed individually. The results are given below and in Table III. It is evident that yields ranged from 58.5 to 69.6%. The over-all average yield is about 64%. This represents about the maximum yield that can be expected from crushing any material from large cakes down to small granules of the desired size.

TABLE III

DATA SHEET FOR CRUSHING CO REAGENT

Cake weight, gm.	Weight fines No. 24, gm.	Weight −(8) +(24), gm.	Yield weight, %
898.2	327.5	570.7	63.7
990.5	347.4	634.5	64.0
1059.7	340.0	611.0	58.5
859.7	282.3	578.5	67.4
1041.9	363.7	661.0	62.2
979.5	351.5	631.0	64.5
996.5	361.5	647.0	65.0
1014.5	352.0	653.0	64.4
1020.0	367.5	652.0	64.0
941.5	326.5	614.5	67.4
968.0	332.0	649.5	67.2
1009.9	359.4	651.5	64.6
1011.0	360.5	649.0	64.2
962.5	353.0	614.5	64.0
761.0	266.0	511.5	68.6
1038.0	371.0	660.5	63.8
1001.5	364.0	636.5	63.5
1090.5	388.5	700.0	64.1
1008.0	374.0	645.0	64.1
1041.5	369.0	668.5	64.1
1062.0	411.5	637.5	60.0
942.5	358.0	596.0	63.4
922.5	322.0	585.5	63.6
910.5	370.0	523.5	57.4
1055.0	397.0	659.0	62.4
997.0	372.0	653.0	65.5
906.0	334.5	578.5	63.9
1006.5	356.0	638.5	63.5
999.5	358.0	681.0	68.2
1001.0	352.0	664.5	66.2
1074.0	406.0	664.5	61.9
915.0	301.0	595.5	66.1
2044.0	669.5	1385.5	67.6
972.0	355.5	623.0	64.1
989.0	338.5	652.0	66.0
1045.5	370.5	676.0	64.6
1032.0	368.5	675.5	65.5
921.0	333.5	619.5	67.3
1020.0	372.0	657.5	64.4
1088.5	382.1	713.8	65.5
1025.5	372.5	674.5	65.6
990.0	347.0	638.5	64.5
1041.0	381.0	722.5	69.6
986.5	372.5	595.0	60.4
1102.5	411.0	700.0	63.5
1062.0	433.0	664.5	62.5

The Effect of Curing and Molding Pressure on Granule Hardness

For the reagent to be suitable for cannister use, it must be hard enough to withstand mechanical shock during packing and actual operating conditions. Two factors were investigated: (1) the effect of curing time of the reagent cake, and (2) the pressure employed to press the cake. It was found that the pressure had no effect on the hardness of the cake as tested by our modified standard

TABLE IV
EFFECT OF CURING TIME ON HARDNESS OF REAGENT GRANULES

Curing time, days	Average hardness
3	69.4
14	75.9
28	79.1

sieve test. The effect of curing time on the granule hardness is given in Table IV. The hardness data shown in the table are average values of the material pressed at 2, 3, 4, and 5 tons per sq. in. It is evident that the hardness of the granules increases with the curing time. From experience in handling other

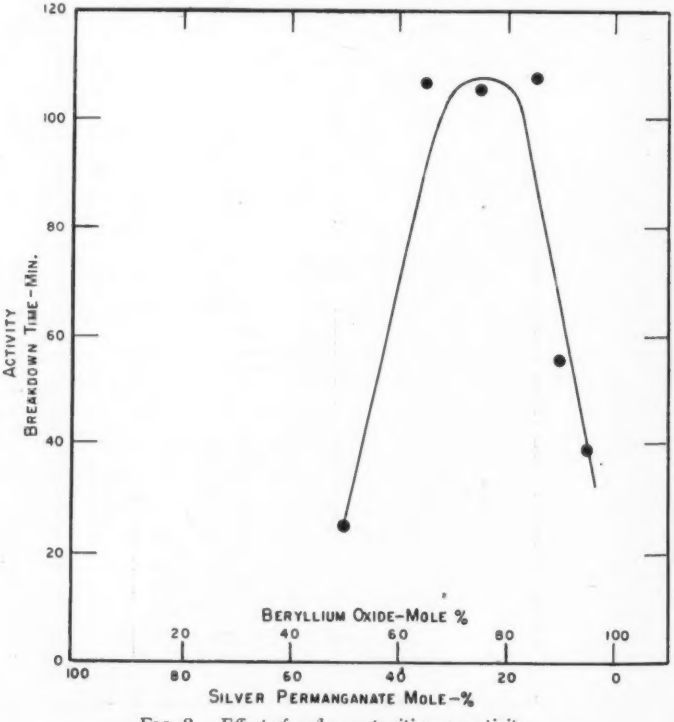

FIG. 2. *Effect of mole composition on activity.*

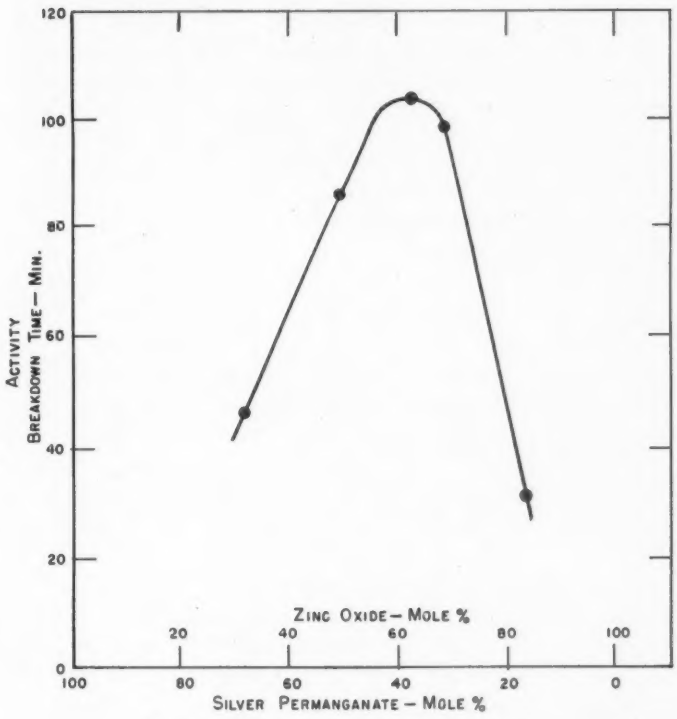

FIG. 3. *Effect of mole composition on activity.*

materials, the granules are not as hard as a good grade charcoal, but from experimental filling of cannisters, the material withstood the handling without crumbling.

Effect of Composition on Activity

From Figs. 2 and 3, it can be seen that an optimum mole concentration of silver permanganate is required to attain maximum activity. In the case of the zinc oxide, the optimum activity lies within the composition range of 63 to 68 mole % of zinc oxide and, in the case of beryllium oxide, 65-68 mole % represents the reagent with optimum activity. From these results and those reported previously (5), it is evident that the oxide carrier has an effect on the amount of silver permanganate required to give maximum activity to a reagent. Further comments on these results are given in the discussion of this report.

Miscellaneous Reagent Mixtures

The effect of depositing silver permanganate on a number of oxides was presented in a previous paper (5). However, a group of new mixtures have been investigated, employing mixtures of oxides and inert salts as carriers, and also

mixtures of metallic oxides without the silver permanganate. A number of other silver salts and metallic oxides were also prepared and studied for activity. The results are given in Table V. With the exception of the reagent prepared from beryllium oxide and silver permanganate, and the three component system containing zinc oxide, ferric oxide and silver permanganate, all of the

TABLE V

CHEMICAL COMPOSITION OF REAGENTS AND THEIR ACTIVITY FOR OXIDIZING CARBON MONOXIDE

Preparation No.	Chemical composition, mole %	Method of preparation	Breakdown time, min. (90% efficiency)
9-A	36% $AgMnO_4$, 64% ZnO	Control	103
27-A	35% $AgMnO_4$, 65% BeO	Same as for $AgMnO_4$-ZnO	107
43-A	33% ZnO-33% MoO_3-33% $AgMnO_4$	"	Nil
24-A	35% Ba $(MnO_4)_2$-65% Zno	"	3
1-Cr-50	31% Ag_2CrO_4-69% ZnO	"	Nil
2-Cr-50	50% $Ag_2Cr_2O_7$-50% ZnO	"	"
3-W-50	50% Ag_2WO_4-50% ZnO	"	"
4-Mo-50	50% Ag_2MoO_4-50% ZnO	"	"
5-W-50	50% $NiWO_4$-50% ZnO	"	"
6-W-50	50% $CuWO_4$-50% ZnO	"	"
7-Cr-50	50% $PbCrO_4$-50% ZnO	"	"
8-Cr-50	50% $CdCrO_4$-50% ZnO	"	"
40-A	50% Ag_2O-50% Co_2O_3	Mechanical mixture	12
20-A	40% Co_2O_3-60% ZnO	H_2O added, mixture pressed	16
19-A	100% $KMnO_4$		Nil
14-A	50% $KMnO_4$-50% MoO_3	H_2O added and pressed	"
18-A	67% $KMnO_4$-33% ZnO	"	"
1-A	33% ZnO-33% MoO_3-33% Al_2O_3	"	"
2-A	33% CuO-33% Fe_2O_3-33% Al_2O_3	"	"
3-A	33% CuO-33% Fe_2O_3-33% TiO_2	"	"
4-A	33% CuO-33% Co_2O_3-33% Al_2O_3	"	"
5-A	33% CuO-33% MoO_3-33% Al_2O_3	"	"
51-A	33⅓% ZnO-33⅓% Fe_2O_3-33% $AgMnO_4$	"	55–34*
52-A	25% ZnO-25% Fe_2O_3-50% $AgMnO_4$	"	89–48*
53-A	16⅔% ZnO-16⅔% Fe_2O_3-67% $AgMnO_4$	"	109–97*

* *Aged 113 hr. at 60°C.*

mixtures investigated were ineffective for the oxidation of carbon monoxide. Although the beryllium oxide and silver permanganate reagent was initially effective in oxidizing carbon monoxide, its aging properties were not as good as the silver permanganate – zinc oxide reagent at room temperature. At a temperature of 60°C. the reagent was completely destroyed in 160 hr. The three component system containing zinc oxide, ferric oxide, and silver permanganate, had the greatest activity and stability of the compounds investigated. However, to prepare a reagent comparable in activity to the control reagent required approximately twice the amount of the costly silver permanganate. Reagent 51-A in the three component system with the same mole % composition of silver permanganate had approximately half the activity of the control preparation No. 9-A.

Discussion

There is no direct evidence to explain the increase in activity of silver permanganate – zinc oxide reagent produced by varying the curing time, molding pressure, and method of preparation. As no physical measurements were made on the reagents in the present investigation, the observed effects can only be discussed by comparing them with results found by other investigators working with catalysts or reagents involving gas – solid reactions. The behavior of the silver permanganate – zinc oxide reagent is similar to that of mixed oxide catalysts or catalysts prepared from oxides deposited on carriers in that they both increase in activity with aging. Both types of mixtures also show a relation between activity and mole composition.

In the case of mixed oxide catalysts and that of salt–oxide mixtures ($BaO - CuSO_4$ and $BaO - ZnSO_4$), it has been postulated by Huttig (3) that compound formation may take place with a resultant increase in catalytic activity. The evidence obtained (3) indicates that the transformation of the mixture into compounds does not occur discontinuously but through individual intermediate states which show no specific X-ray diagram. It would be expected that a reaction of this type would take place over long periods of time of the same order of magnitude as aging or curing times necessary to obtain optimum activity of the catalysts or reagents.

It is of interest also to point out that an increase in molding pressure or a method of preparation which gives the most intimate mixture of the reagents would enhance the probability of compound formation.

It is known that granule size, type of carrier, and mole composition have an effect on the activity of the silver permanganate reagent (4, 5). Of these, the influence of mole composition would support the theory that compound formation may take place. A study of the chemical composition and decomposition products by chemical and X-ray analysis of the silver permanganate – zinc oxide reagent is at present under investigation (7).

References

1. Berkman, S., Morrell, J. C., and Egloff, G. Catalysis. 2nd ed. Reinhold Publishing Corporation, New York. 1946.
2. Grant, G. A., Katz, M., and Haines, R. L. Can. J. Technol. 29: 43-51. 1951.
3. Huttig, G. F. Discussions of Faraday Society. No. 8, 215-222. 1950.
4. Katz, M., Grant, G. A., and Riberdy, R. Can. J. Research, B, 28: 799-814. 1950.
5. Katz, M. and Halpern, S. Ind. Eng. Chem. 42: 345-352. 1950.
6. Katz, M. and Katzman, J. Can. J. Research, F, 26: 318-330. 1948.
7. Katz, M., Wilson, L. G., and Riberdy, R. In preparation.

A SYRINGE-HEAD FOR ATTACHMENT OF GLASS CAPILLARY NEEDLES TO GLASS SYRINGES[1]

By G. E. Bucher[2] and R. D. Bradfield[3]

Abstract

A new method is described for attaching glass capillary injection needles to commercial tuberculin syringes, without the use of rubber or plastic tubing. The attachment is made by means of a slip-on metal syringe-head, which fits the syringe in place of a commercial steel needle. The capillary needle passes through the adapter head and is held in place by a rubber gasket under pressure exerted by a metal disk and a screw-cap.

The use of fine capillary glass tubing for microinjection needles to replace the much coarser commercial steel needles has confronted investigators with the problem of connecting the needle to the syringe. Since most common methods of joining needle to syringe are cumbersome, it is hoped that a description of this new attachment will be useful to those engaged in injection techniques employing glass capillary needles drawn to a fine point.

The attachment may be considered as a slip-on metal syringe-head which connects the needle to the syringe by a leakproof joint. The syringe-head consists of four parts, which are shown in diagrammatic section (Fig. 1). The

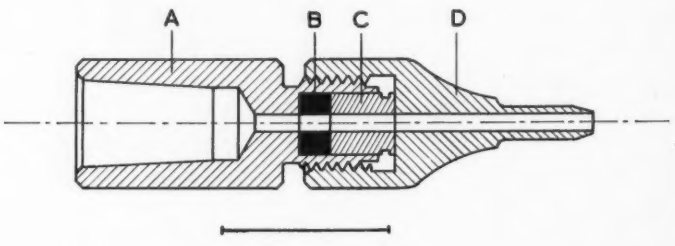

FIG. 1. *Diagrammatic cross section of the syringe-head drawn to scale. A, basal portion; B, rubber disk; C, metal disk; D, cap.*

basal portion (A) is bored with a standard taper to receive the tapered end of a Luer syringe in the same manner as an ordinary steel needle. Distally, the basal portion is excavated to receive a soft rubber disk (B) and a metal disk (C). The metal disk is bored centrally to allow the glass capillary needle to pass through into the basal portion; similarly the rubber disk is pierced. When

[1] *Manuscript received August 13, 1951.*
Contribution No. 2758, Division of Entomology, Science Service, Department of Agriculture, Ottawa. Canada.
[2] *Agricultural Research Officer, Biological Control Investigations Laboratory, c/o Department of Bacteriology, Queen's University, Kingston, Ont.*
[3] *Instrument Maker, Queen's University, Kingston, Ont.*

assembled, the metal disk (C) projects beyond the lip of the basal portion. The cap (D) is threaded to engage with the threads of the basal portion. When tightened, it bears on the metal disk, which in turn compresses the rubber disk and causes the latter to grip the glass capillary and form a watertight seal. Although considerable pressure may develop in a syringe if the capillary needle has been drawn out to a very fine orifice, leakage from the tapered joint between basal portion and syringe is prevented by a light coating of silicone stopcock grease. The metal parts of the syringe-head have been milled from German silver, because this is easier to work with than stainless steel. This material satisfactorily resists ordinary tarnishing and corrosion. A photograph of the disassembled head is shown in Fig. 2. The end of the cap may be split and threaded to take another secondary cap, which provides a second point of attachment of the glass capillary. In practice this has been found to be an unnecessary refinement.

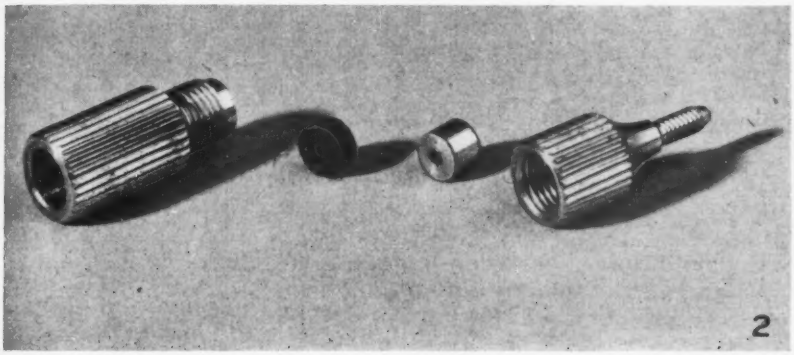

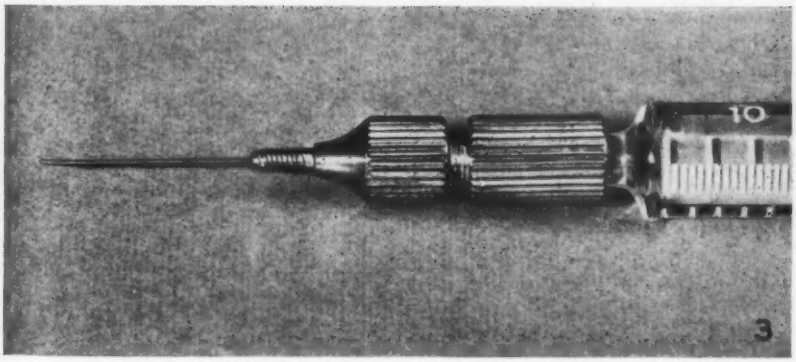

FIG. 2. *Syringe-head broken down into its four components.*
FIG. 3. *Tuberculin syringe, head, and capillary needle assembled.*

In order to test the pathogenicity of microorganisms to insects by the injection method the instruments employed must satisfy certain requirements. The needles must be fine to avoid injury and excessive bleeding. Commercial steel needles are too coarse for most insects. The instruments must be numerous since a series of tests at different dilutions are performed at one time, each requiring a separate sterile needle and syringe. Frequently, only small amounts are available for injection, so that attachment of needle to syringe must be made without the use of a connecting tube and a large needle base. The equipment must be readily sterilized and easy to assemble in a sterile condition. The syringe assembly must be capable of delivering an accurately measured small dose. For all practical purposes the 1/2 or 1/4 cc. tuberculin syringe, whose plunger is depressed by one of the numerous screw-thread activators on the market, has sufficient accuracy. The syringe-head was designed specifically to facilitate the injection into insects of small quantities of liquids bearing pathogenic organisms. It meets the requirements mentioned above in that it allows the attachment of a small glass capillary needle directly to the syringe without connecting tubing to increase the necessary volume of inoculating fluid; it can be made cheaply in quantity and fitted to a series of tuberculin syringes; it is readily cleaned and sterilized, and syringe, syringe-head, and capillary needle are easily assembled in a sterile condition.

In practice, syringe, syringe-head, and needle are sterilized separately. The syringe is filled with the injection fluid and the tapered end is lightly greased. The syringe-head is fitted to the syringe, the capillary needle thrust through the head to meet the syringe, and the cap of the head tightened firmly to grip the needle. The needle is then drawn out to a fine point in a microflame. Depressing the plunger of the syringe expels the air in the needle, and the syringe assembly is ready for use. Fig. 3 shows the syringe, head, and injection needle mounted for use.

The principle of connecting a glass needle to a syringe by means of a rubber gasket tightened by a screw-cap is not new. Bergold (1) used an identical method to fix a glass needle to his stainless steel syringe, which was designed specifically for inoculation of insects. In Bergold's apparatus, the basal part of the head was an integral part of the body of the syringe itself. The high cost of manufacture of these complete steel syringes is prohibitive where conditions demand that a number of instruments be available and ready for action at the same time. The new metal syringe-heads are relatively inexpensive and have the added advantage that they can be used in conjunction with commercial glass tuberculin syringes.

Reference

1. BERGOLD, G. Biol. Zentr. 61: 158-162. 1941.

AUTOXIDATION OF METHYL ESTERS OF PEANUT OIL FATTY ACIDS

THE EFFECTS OF INCUBATION TEMPERATURE AND OF ADDED IRON ON INFRARED ABSORPTION SPECTRA AND ON OTHER CHANGES[1]

By H. W. Lemon, Elizabeth M. Kirby, and Ruth M. Knapp

Abstract

The infrared absorption spectra of methyl esters of peanut oil fatty acids showed changes principally in three regions during incubation at temperatures from 22° to 100°C. In the −OH stretching region (3730–3005 cm.$^{-1}$) a band developed in the early stages of autoxidation which was believed to be associated with the formation of hydroperoxides. Later two bands, probably associated with the decomposition of hydroperoxides to other compounds containing hydroxyl groups, appeared at higher wave numbers. Increased temperature of incubation accelerated the formation and decomposition of peroxides, and the presence of iron stearate catalyzed only their decomposition. In the C = 0 stretching region (1840–1630 cm.$^{-1}$) three bands appeared at different stages of autoxidation. In the third region (1130–740 cm.$^{-1}$) two of the bands formed were assigned to diene conjugation and to *cis* to *trans* isomerization. Some separation of absorbing compounds was effected by molecular distillation and by countercurrent extraction of autoxidized samples.

Introduction

The purpose of this investigation was to study the changes that occur in the infrared absorption spectra of methyl esters of peanut oil fatty acids during autoxidation, and to relate them where possible to chemical analyses, especially to peroxide determinations. The effects of the temperature of incubation and of the presence of dissolved iron stearate upon these changes were noted.

In preliminary infrared studies it was found that increased absorption due to autoxidation occurred principally in three regions of the spectrum, namely, (I) 3730 to 3005 cm.$^{-1}$, (II) 1840 to 1630 cm.$^{-1}$, and (III) 1130 to 740 cm.$^{-1}$. Absorption in the first and second regions is associated with the presence in the molecule of hydroxyl and carbonyl groups respectively. It is known that double bonds having a *trans* configuration, and diene or triene conjugated systems contribute to the absorption in the third region.

Infrared spectrophotometry, as a means of studying the autoxidation of oils and related substances, has been used to a limited extent in recent years. Dugan, Beadle, and Henick (8) determined the absorption spectrum of autoxidized methyl linoleate in the hydroxyl and carbonyl regions. They reported the development of absorption bands with maxima at 3430, 3470, and above 3500 cm.$^{-1}$ in the first region and assigned these to hydroperoxides, to molecular hydroxyl content, and to the potassium iodide reduction product of the autoxidized ester, respectively. In the second region they found absorption

[1] *Manuscript received August 15, 1951.*
Contribution from the Department of Biochemistry, Ontario Research Foundation, Toronto, Ont., with financial assistance from the National Research Council of Canada.

bands with maxima at 1724 and 1733 cm.$^{-1}$. Honn, Bezman, and Daubert (16) studied increased absorption of autoxidizing linseed oil in the hydroxyl region and developed a method for determining the carboxyl, hydroperoxide, and R-OH fractions from chemical and infrared measurements. They also reported increased absorption at 10.2 μ (980 cm.$^{-1}$) due to autoxidation. Shreve, Heether, Knight, and Swern (26) made a detailed study of the absorption of peroxides and hydroperoxides and concluded that peroxides absorb specifically between 1000 and 833 cm.$^{-1}$. Henick (14) found a band in the hydroxyl region in the deodorization distillates of oxidized milk fat and found several bands in the carbonyl region which were associated with flavor changes. Knight, Eddy, and Swern (18) reported increased absorption in the region from 2.8 to 2.9μ (3571-3448 cm.$^{-1}$) on autoxidation of methyl oleate. Their paper was chiefly concerned with the formation of *trans* isomers, followed by measuring the intensity of the infrared band at 10.31μ (970 cm.$^{-1}$) in the early stages of autoxidation. Cole and Field (6) studied the infrared spectra of oxidized GR-S and other elastomers and found increased absorption in each of the three regions.

Materials and Methods

The substrates used for the autoxidation experiments were distilled methyl esters of peanut oil fatty acids, with and without 10 p.p.m. added iron, prepared as described previously (19).

Peroxide values were determined as milliequivalents of oxygen per 1000 gm. of esters, using a micromodification of the method of Wheeler (30). Approximately 0.2 gm. of the sample was weighed into a 1 ml. beaker which was placed in an iodine flask. To this was added 2.5 ml. of the chloroform – glacial acetic acid solvent, then 0.5 ml. of saturated aqueous potassium iodide solution. This was mixed for one minute, 2.5 ml. of distilled water added, and the liberated iodine titrated with 0.01 *N* sodium thiosulphate using a starch indicator.

Iodine values and free fatty acids were determined according to the official methods of the American Oil Chemists' Society (2).

Ultraviolet absorption studies were made in the region from 220 to 272 mμ using a Beckman quartz spectrophotometer. Isooctane, purified by passage through a column of silica gel (12), or 95% ethanol, purified by refluxing in the presence of zinc dust and potassium hydroxide for six hours prior to distillation, was used as solvent.

The infrared absorption spectra were recorded with a Perkin-Elmer, Model 12C, spectrometer, a-c. operation, equipped with interchangeable sodium chloride and calcium fluoride prisms. Maximum resolution was obtained with slow operating speeds and narrow slits. The slit drive was used for recording the complete spectra and for regions II and III. Conditions of amplification were set so that full scale deflection was obtained in all regions, and amplifier noise was not a significant factor in analytical accuracy, although it varied in the different regions.

Sample cells employed for the work were of conventional design and consisted of rock salt plates separated by lead spacers.

When solution of the sample was necessary, carbon disulphide was used as solvent, and the solution concentrations are indicated on the accompanying graphs.

Optical density $\left(\log \frac{I_0}{I}\right)$ measurements of all autoxidized samples were based on differential absorption in the same cell, with the unoxidized sample as the I_0 curve. For density measurements of the unoxidized esters, with and without addition of free fatty acids, a "no-cell" background was used as the I_0 curve.

Experimental

Approximately 100 gm. of the esters was placed in 180 ml. electrolytic beakers. Methyl esters without iron were incubated at 22°, 40°, 60°, 80°, and 100°C., and methyl esters with added iron at 22°, 60°, and 100°C. Two ml. was withdrawn from each beaker for chemical and spectrophotometric analyses weekly for 10 weeks, then at 12, 14, 16, 18, 20, 26, and 32 weeks. The esters that were incubated at 80° and 100°C. were transferred to a refrigerator after 13 weeks as autoxidation was well advanced. Peroxide values, iodine values, and free fatty acids were determined, color changes noted, diene conjugation measured, and a detailed study of the infrared absorption in three regions of the spectrum was made. The infrared spectrum for a sample of the unoxidized methyl esters containing 5% of peanut oil fatty acids, as well as that for the unoxidized esters alone, was determined to see what effect the increase in free fatty acids during autoxidation had on absorption.

To effect some separation of autoxidation products and of infrared absorbing substances, samples incubated for 13 weeks at 100°C. with and without added iron were subjected to high-vacuum distillation at 125° to 160°C. using a flask similar to that illustrated in a paper by Hickman and Sanford (15, Fig. 6). This roughly separated unpolymerized from polymerized esters; the esters with no added iron yielded 42% residue and 58% distillate, whereas the esters with 10 p.p.m. added iron yielded 47% residue and 53% distillate.

A total of 4.341 gm. of the same autoxidized esters with no added iron was fractionated also by means of a Craig countercurrent solvent extractor (7). Five extractions were made, using hexane and 80% ethanol in water, and each time the contents of the 25 extraction tubes were combined into four fractions on the basis of weight distribution. Fractions 1, 2, 3, and 4 represented tubes 0 to 7, 8 to 11, 12 to 18, and 19 to 24. The total weights obtained from the five extractions were 3.279, 0.168, 0.222, 0.248 gm. respectively, equivalent to a recovery of approximately 90% of the original esters.

Infrared and ultraviolet absorption of all the above fractions were determined.

Results and Discussion

As autoxidation proceeded, certain progressive changes were observed.

The most obvious was a change in color particularly in the esters with added iron. The samples containing no iron became yellow, then amber, and then darkened further with increased time and temperature of incubation. At any given time and temperature, however, the samples containing iron were darker in color than those with no iron. Better and Davidsohn (4) observed a darkening of soaps by metals and used this as a measure of the catalytic power of the metal.

Iodine values decreased and free fatty acids increased progressively with autoxidation; both trends are well known phenomena. Table I shows the changes that occurred in one of the samples studied.

TABLE I

CHANGES IN IODINE VALUES, FREE FATTY ACID CONTENT, AND PEROXIDE VALUES, UPON INCUBATION OF METHYL ESTERS OF PEANUT OIL FATTY ACIDS AT 60°C.

Time of incubation, weeks	Iodine value	Free fatty acids, % oleic acid	Peroxide value, m.e. per 1000 gm.
0	98.6	0.2	4
2	90.3	0.3	221
4	87.1	0.4	364
6	85.4	0.9	568
8	81.4	1.7	539
10	75.1	2.4	499
12	72.7	3.3	421
14	69.3	3.5	168
16	65.5	4.2	182
18	60.7	5.2	191
20	54.6	7.5	160
26	49.0	7.8	138
32	40.5	9.9	75

Peroxide values were markedly affected by the temperature of autoxidation. At higher temperatures the rate of increase of peroxide values was accelerated, the maximum realized was lower, and the decline was initiated sooner. Fig. 1 shows the rise and subsequent decline of peroxide values at temperatures from 22° to 100°C. Other workers have reported similar results (1, 13, 17, 20, 24, 28). At 80° and 100°C. the peroxide value dropped to a constant value in the late stages of autoxidation; it has been suggested by various workers that this may be due to the existence of different types of peroxides, some being more heat-stable than others (20, 23, 25).

Table II gives the maximum peroxide values and the time required to reach the maxima. It has been suggested that the maximum peroxide content realized is a function of the temperature of autoxidation (17).

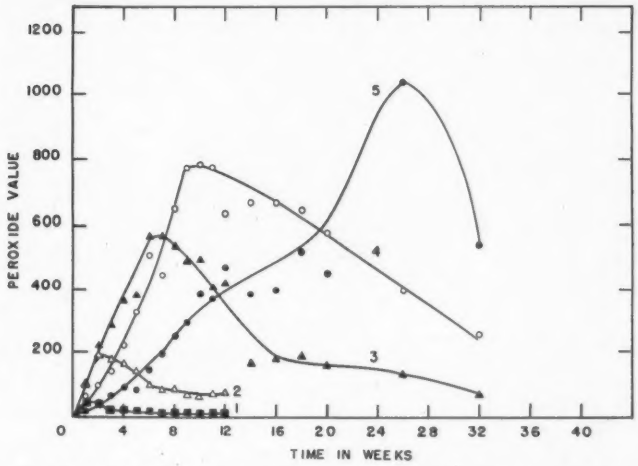

FIG. 1. *The effect of incubation temperature upon the peroxide value of methyl esters of peanut oil fatty acids; (1) incubation at 100°C., (2) at 80°C., (3) at 60°C., (4) at 40°C., (5) at 22°C.*

TABLE II

THE EFFECT OF TEMPERATURE OF INCUBATION UPON THE MAXIMUM PEROXIDE CONTENT REALIZED AND THE TIME REQUIRED

Methyl esters of peanut oil fatty acids	Temperature of incubation	Maximum peroxide value, m.e. per 1000 gm.	Time required to reach maximum peroxide value, weeks
Esters	22°C.	1042	26
Esters + 10 p.p.m. iron	22°C.	819	26
Esters	40°C.	778	10
Esters	60°C.	568	6
Esters + 10 p.p.m. iron	60°C.	419	6
Esters	80°C.	199	2
Esters	100°C.	49	2
Esters + 10 p.p.m. iron	100°C.	44	1

Fig. 2 shows the effect of dissolved iron stearate upon peroxide formation and decomposition at 60°C. The presence of iron did not accelerate the formation of peroxides significantly, but rather seemed to promote peroxide decomposition. The catalytic effect of iron and other metals on autoxidation is well known. Farmer *et al.* (9, 10) have pointed out that iron salts can play a dual role of peroxidation promoters and peroxidation destroyers. According to Lundberg (22), metallic pro-oxidants exert their effect by catalyzing the decomposition of peroxides to form free radicals, thus initiating new reaction chains.

The development of diene and triene conjugation during autoxidation of polyunsaturated fatty acids and esters was first reported by Farmer, Koch,

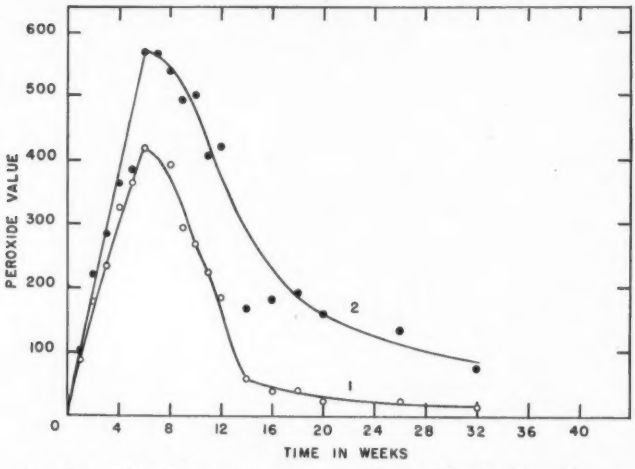

FIG. 2. *The effect of dissolved iron stearate upon the peroxide value of methyl esters of peanut oil fatty acids incubated at 60°C.; (1) methyl esters + 10 p.p.m. added iron, (2) control methyl esters.*

and Sutton (11) and by Bolland and Koch (5). More recent work has been reviewed by Swern, Scanlan, and Knight (29), Lundberg (21), and Sims (27). In view of the correlation between conjugation and peroxidation, diene conjugation in the samples of autoxidized peanut oil methyl esters was determined by measuring the ultraviolet absorption at 232 mμ which was the wave length of maximum absorption in the early stages of autoxidation. Conjugation increased to a maximum, then declined in a manner closely parallel with the rise and decline of peroxide values. The higher the temperature of autoxidation, the lower was the maximum conjugation. These results are in agreement with those of Allen, Jackson, and Kummerow (1), Bergstrom and Holman (3), Gunstone and Hilditch (13), and of Hess and O'Hare (17). Later the point of maximum absorption shifted gradually to shorter wave lengths and was finally obliterated by a marked general increase in absorption in this region. The presence of added iron in the esters had little or no effect on diene conjugation.

The ultraviolet absorption curves of fractions obtained by molecular distillation and by countercurrent extraction from esters that were incubated for 13 weeks at 100°C. resembled those of the highly autoxidized samples.

The results of infrared absorption studies in the three spectral regions will be discussed separately.

Infrared Region I (3730-3005 cm.$^{-1}$)

Absorption in the hydroxyl region by the unoxidized methyl esters of peanut oil fatty acids and by the same esters containing 5% of free fatty acids from peanut oil is shown in Fig. 3, Curves 1 and 2. The latter curve shows increased absorption between 3400 and 3000 cm.$^{-1}$ caused by the addition of free fatty acids.

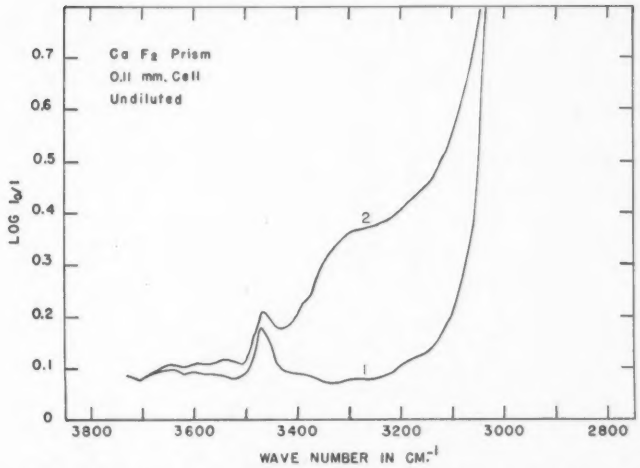

FIG. 3. *Infrared absorption in the hydroxyl region by unoxidized methyl esters of peanut oil fatty acids (Curve 1) and by the same esters containing 5% free fatty acids prepared from peanut oil (Curve 2).*

Fig. 4 shows changes that occurred during the incubation of the esters at 60°C. and Fig. 5 illustrates the effect of the temperature of incubation upon the formation of infrared absorption bands in this region. The most outstanding change in absorption in the early stages of autoxidation was the development of a band with maximum absorption at 3425 cm.$^{-1}$, believed to be associated

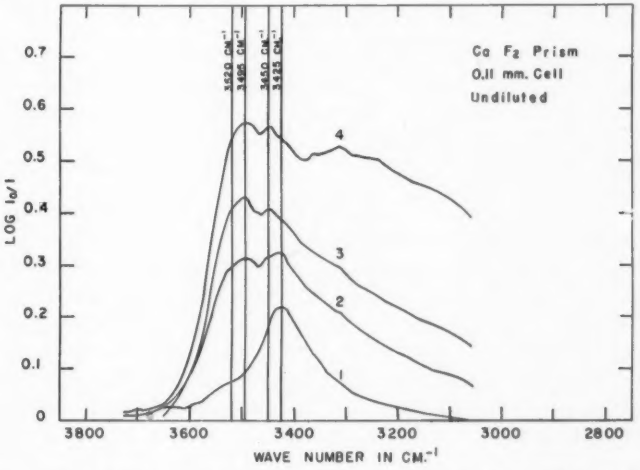

FIG. 4. *Increased infrared absorption in the —OH stretching region caused by autoxidation of methyl esters of peanut oil fatty acids at 60°C.; (1) incubated for 4 weeks, (2) for 12 weeks, (3) for 18 weeks, (4) for 32 weeks.*

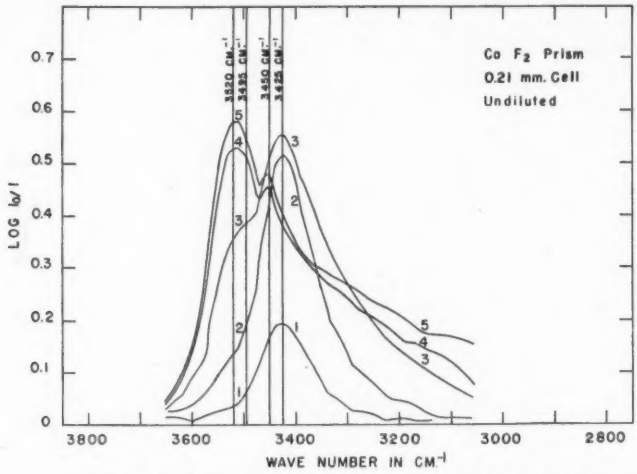

FIG. 5. *Increased infrared absorption in the —OH stretching region by methyl esters of peanut oil fatty acids incubated for eight weeks; (1) at 22°C., (2) at 40°C., (3) at 60°C., (4) at 80°C., (5) at 100°C.*

in part at least with the formation of hydroperoxides. Absorption at 3425 cm.$^{-1}$ increased with increasing peroxide values although the relationship was not one of direct proportionality. Dugan, Beadle, and Henick (8) found a similar band at 3430 cm.$^{-1}$ in the spectrum of autoxidized methyl linoleate, which they related to hydroperoxides. Honn, Bezman, and Daubert (16) and Knight, Eddy, and Swern (18) also related increased absorption in this region to hydroperoxides.

When the esters were incubated at 22°C. the 3425 cm.$^{-1}$ band was faintly evident after one week. After 32 weeks it had become very intense and was the only strong band observed. In autoxidations at higher temperatures the development of the band at 3425 cm.$^{-1}$ was more rapid in the initial stages (Fig. 5, Curves 1, 2, and 3) but the maximum intensity reached was inversely related to the temperature of incubation.

The second absorption band to appear was first observed as a shoulder on the side of the 3425 cm.$^{-1}$ band (Fig. 4, Curve 2 and Fig. 5, Curve 3). It was evident after one week in the spectra of esters incubated at 100° and 80°C., after three weeks at 60°C., and after five weeks at 40°C. It was faintly evident after 32 weeks at 22°C. Maximum absorption was initially at about 3520 cm.$^{-1}$ but gradually shifted to 3495 cm.$^{-1}$. The intensity of absorption increased throughout the autoxidation and the rate of increase was greater at higher temperatures (Fig. 5, Curves 4 and 5).

Shortly after peroxide values had reached their maximum, another weak shoulder was observed on the side of the 3425 cm.$^{-1}$ band, and later became resolved at 3450 cm.$^{-1}$. This band is seen in Curves 3 and 4 of Fig. 4 and Curves

4 and 5 of Fig. 5. The 3425 cm.$^{-1}$ band was obliterated by the increase in the intensity of the bands at 3450 and 3495 cm.$^{-1}$, which are probably associated with the breakdown of hydroperoxides to other substances containing —OH groups.

In highly autoxidized samples there was also a broad band below 3365 cm.$^{-1}$ (Fig. 4, Curve 4), which was probably due to the increase in the free fatty acid content.

The presence of dissolved iron stearate catalyzed the formation of the substance responsible for the second peak at 3520 cm.$^{-1}$ when esters were incubated at 60° and 100°C. and Fig. 6 shows this effect. After one week at 100°C. the absorption of the sample without iron (Curve 1) showed maxima at 3425 and 3520 cm.$^{-1}$ of approximately equal intensities. However, Curve 2 for the sample with added iron showed the band at 3520 cm.$^{-1}$ to be more intense and the band at 3425 cm.$^{-1}$ to be almost nonexistent. After eight weeks at 60°C.

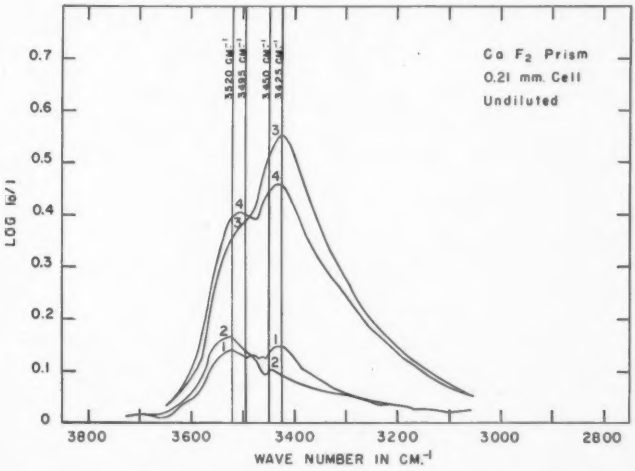

FIG. 6. *Increased infrared absorption in the —OH stretching region caused by autoxidation of methyl esters of peanut oil fatty acids, with and without iron; (1) control esters incubated for one week at 100°C., (2) esters with 10 p.p.m. iron incubated for one week at 100°C., (3) control esters incubated for 8 weeks at 60°C., (4) esters with 10 p.p.m. iron incubated for eight weeks at 60°C.*

the optical density at 3520 cm.$^{-1}$ for the sample without iron (Curve 3) was less than that of the same sample with added iron (Curve 4), whereas at 3425 cm.$^{-1}$ it was greater. These results are in agreement with those illustrated in Fig. 2 where it was shown that at 60°C. the iron catalyzed the decomposition rather than the formation of peroxides.

The absorption in this region of the distillates and residues obtained by distillation of the esters, with and without iron, incubated at 100°C. for 13 weeks, is shown in Fig. 7. Curves 3 and 4 for the undistilled esters show mainly

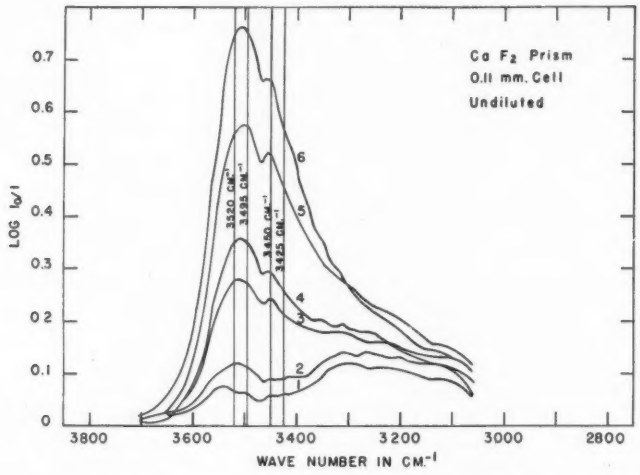

FIG. 7. *Increased infrared absorption in the —OH stretching region by fractions obtained by distillation of esters incubated for 13 weeks at 100°C.; (1) distillate from esters containing 10 p.p.m. iron, (2) distillate from control esters, (3) undistilled esters containing iron, (4) undistilled esters without iron, (5) residue from esters containing iron, (6) residue from control esters.*

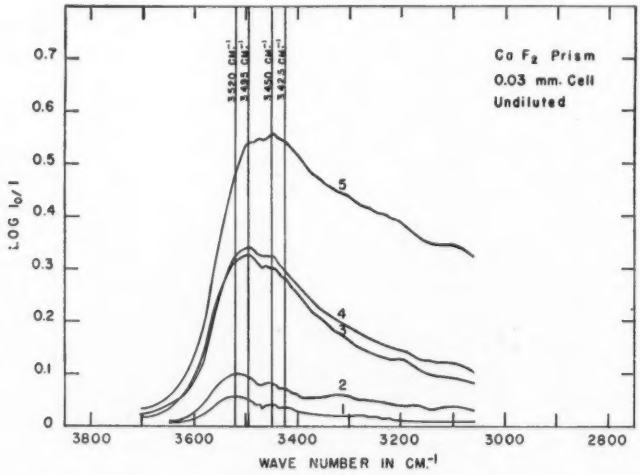

FIG. 8. *Increased infrared absorption in the —OH stretching region by fractions obtained by countercurrent extraction of esters incubated for 13 weeks at 100°C.; (1) Fraction 1, (2) unfractionated esters, (3) Fraction 2, (4) Fraction 3, (5) Fraction 4.*

bands at 3510 cm.$^{-1}$ and 3450 cm.$^{-1}$. Most of this absorption was found to be in the residues after distillation. The distillates showed greatest absorption below 3305 cm.$^{-1}$ probably due to free fatty acids. In all cases the absorption was lower when iron was added to the original esters.

The absorption in this region of the four fractions yielded by the Craig countercurrent extraction apparatus are shown in Fig. 8. Fraction 1 presented the same absorption curve in this region as the sample before extraction except that absorption was weaker. The curves for Fractions 2 and 3 were almost identical, and similar to the untreated sample, indicating a concentration of absorbing substances in these samples. Fraction 4 showed still greater concentration of the absorbing substances, particularly of those responsible for absorption at 3450 cm.$^{-1}$.

Infrared Region II (1840-1630 cm.$^{-1}$)

Absorption in the carbonyl region by the unoxidized methyl esters and by the same esters containing 5% of free fatty acids is shown in Fig. 9, Curves 1 and 2. The latter curve shows a band with maximum at 1710 cm.$^{-1}$ as well as the strong ester carbonyl band.

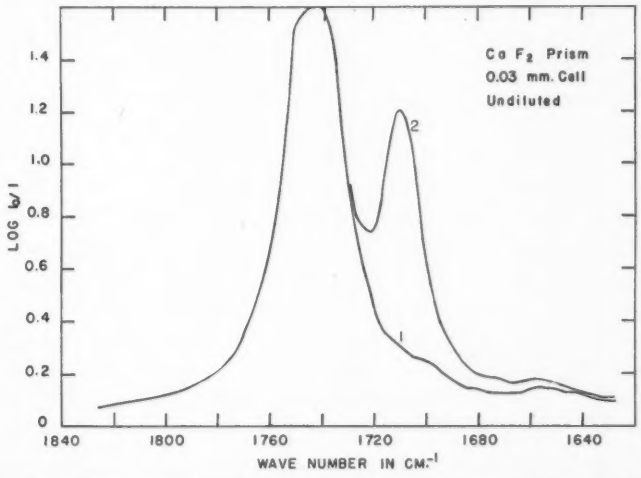

FIG. 9. *Infrared absorption in the C = O stretching region by unoxidized methyl esters of peanut oil fatty acids (Curve 1) and by the same esters containing 5% free fatty acids from peanut oil (Curve 2).*

Changes in absorption that occurred in this region during autoxidation of the methyl esters were presumably due to the formation of substances containing carbonyl or carboxyl groups and are shown in Fig. 10. The most noticeable change was the development of a band with maximum absorption between 1721 and 1727 cm.$^{-1}$, which, on the original record, appeared as a shoulder on the side of the ester carbonyl band. Dugan, Beadle, and Henick (8), using a

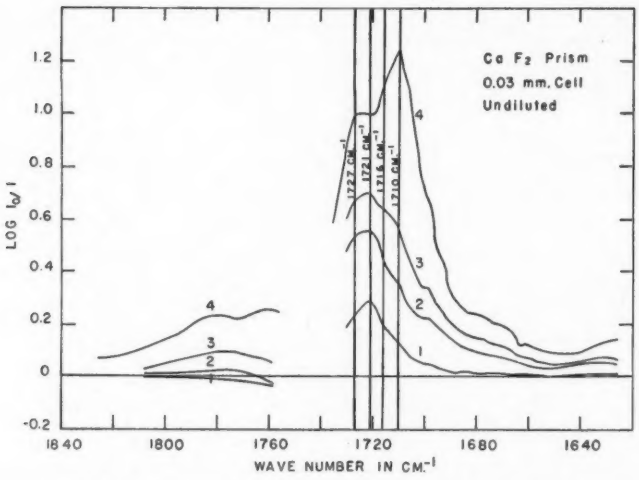

FIG. 10. *Increased infrared absorption in the C = O stretching region caused by autoxidation of methyl esters of peanut oil fatty acids; (1) incubated for 20 weeks at 22°C., (2) for 20 weeks at 40°C., (3) for 20 weeks at 60°C., (4) for 32 weeks at 60°C.*

lithium fluoride prism, found a doublet in this region in the spectrum of autoxidized methyl linoleate with maxima at 1724 and 1733 cm.$^{-1}$, but in the present work only one band was observed. It was faintly evident after incubation for one week at 22°C. and was well formed after eight weeks. The intensity of absorption increased throughout the period of incubation, and, as is shown in Fig. 10, was greater when incubation was done at higher temperatures.

After prolonged incubation at 40° and 60°C. a fairly strong peak at 1710 cm.$^{-1}$ was noted, presumably caused by the increase in free fatty acids. Also there was some indication of a band at 1716 cm.$^{-1}$ in the spectra of highly autoxidized samples. It was present as a shoulder on the 1721-1727 cm.$^{-1}$ band after the samples were incubated for 20 weeks or more at 60°C. or for 26 weeks at 40°C. It is more clearly evident in the curve for the esters incubated for 13 weeks at 100°C. (Fig. 11, Curve 3).

The presence of added iron in the esters had no detectable effect upon infrared absorption in this region.

The absorption curves of the residues and distillates obtained by the molecular distillation of esters, with and without added iron, incubated for 13 weeks at 100°C. are shown in Fig. 11. Curve 3 for the undistilled esters showed the bands at 1721 and 1716 cm.$^{-1}$ as well as evidence of a band below 1716 cm.$^{-1}$. Curves 1 and 2 show absorption by the distillates from esters incubated with and without added iron, respectively, and these samples showed maxima at 1721 and 1710 cm.$^{-1}$. Curves 4 and 5 for the residues from esters without and with added iron respectively, had absorption peaks at 1721 and 1716 cm.$^{-1}$.

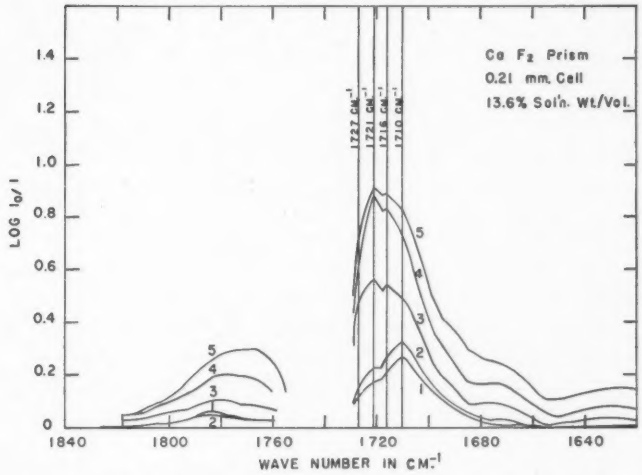

FIG. 11. *Increased infrared absorption in the C = O stretching region by fractions obtained by distillation of esters oxidized for 13 weeks at 100°C.; (1) distillate from esters containing 10 p.p.m. iron, (2) distillate from control esters, (3) undistilled esters without iron, (4) residue from esters without iron, (5) residue from esters containing iron.*

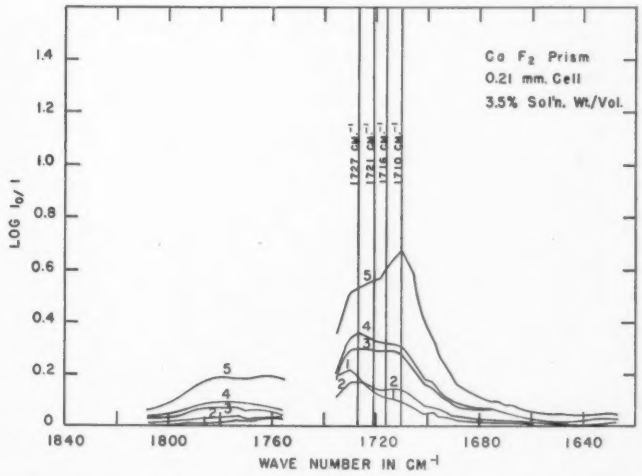

FIG. 12. *Increased infrared absorption in the C = O stretching region by fractions obtained by countercurrent extraction of esters incubated for 13 weeks at 100°C.; (1) Fraction 1, (2) unfractionated esters, (3) Fraction 2, (4) Fraction 3, (5) Fraction 4.*

These results show that most of the substances responsible for infrared absorption in this region were concentrated in the residues, with the exception of that substance, believed to be free fatty acids, which caused the absorption at 1710 cm.$^{-1}$.

Infrared absorption curves of the fractions obtained by countercurrent extraction of methyl esters incubated for 13 weeks at 100°C. are given in Fig. 12. Curve 2 represents the absorption of the unextracted sample which showed the main band at 1727 cm.$^{-1}$ and a single broad band, presumably caused by a combination of the bands at 1710 and 1716 cm.$^{-1}$. Fraction 1 (Curve 1) absorbed more strongly above 1727 cm.$^{-1}$ than the unextracted sample, but absorption was weaker at other parts of the absorption curve. Curves 3 and 4 show that Fractions 2 and 3 had almost identical infrared spectra, and Curve 5 shows that absorption by Fraction 4 was concentrated at 1710 cm.$^{-1}$. Fraction 4 and the distillates, discussed above, probably contain the free fatty acids developed during autoxidation.

Infrared Region III (1130-740 cm.$^{-1}$)

Absorption in this region by the unoxidized methyl esters and by the same esters containing 5% free fatty acids is shown in Fig. 13, Curves 1 and 2. Curve 2 shows increased absorption between 980 and 880 cm.$^{-1}$ caused by the addition of free fatty acids.

The principal changes in absorption that occurred on autoxidation of the methyl esters are shown in Fig. 14. The first band to appear had maximum absorption at 988 cm.$^{-1}$ and was evident in all samples after incubation for one week. It is believed to be related to the development of diene conjugation.

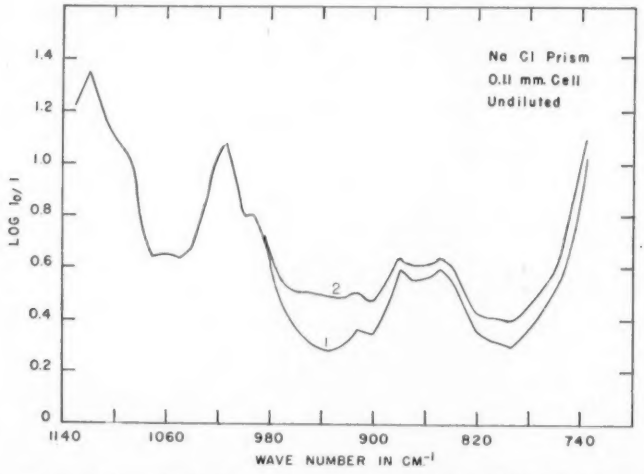

FIG. 13. *Infrared absorption in the third region by unoxidized methyl esters of peanut oil fatty acids (Curve 1) and by the same esters containing 5% free fatty acids from peanut oil (Curve 2).*

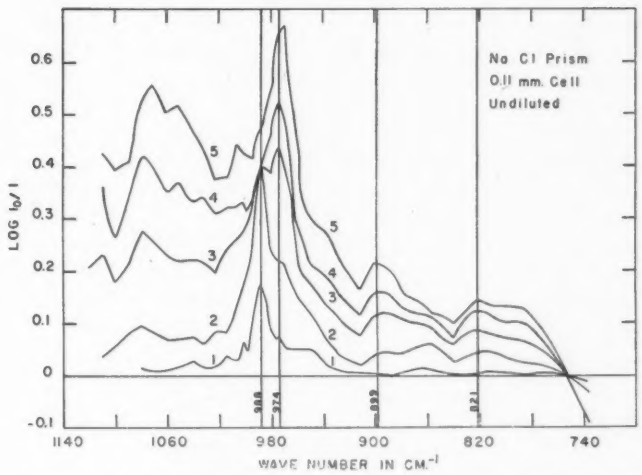

FIG. 14. *Increased infrared absorption by methyl esters of peanut oil fatty acids, incubated for 10 weeks, (1) at 22°C., (2) at 40°C., (3) at 60°C., (4) at 80°C., (5) at 100°C.*

At an incubation temperature of 22°C. this band steadily increased in intensity throughout the 32 week period, but at higher temperatures absorption reached a maximum value inversely related to the temperature of incubation, as is shown in Table III. There was a close relationship between absorption at 988 cm.$^{-1}$, ultraviolet absorption at 232 mμ, peroxide values, and absorption at 3425 cm.$^{-1}$ in the hydroxyl region.

A second band with maximum absorption at about 974 cm.$^{-1}$, believed to be due to the formation of isomers containing *trans* double bonds, was evident

TABLE III

EFFECT OF INCUBATION TEMPERATURE AND OF TIME ON ABSORPTION AT 988 CM.$^{-1}$ (DIENE CONJUGATION)

Time in weeks	Incubation temperatures				
	22°C.	40°C.	60°C.	80°C.	100°C.
	$\log \frac{I_0}{I}$				
2	0.04	0.10	0.18	0.19	0.22
4	0.07	0.20	0.29	0.26	
8	0.13	0.36	0.39		
10	0.18	0.40	0.40		
12	0.23	0.48			
16	0.30	0.58			
20	0.38	0.59			
26	0.55				
32	0.64				

after one week of incubation at temperatures of 40°C. and higher, but in the early stages of autoxidation it was weak. After 32 weeks' incubation at 22°C. it was just becoming established as a shoulder on the much stronger 988 cm.$^{-1}$ band, but at higher incubation temperatures it developed more rapidly, increased in intensity throughout the period of incubation, became more intense than the 988 cm.$^{-1}$ band, and eventually completely obscured it. The effect of temperature of incubation and of time on its development are shown in Table IV. Knight, Eddy, and Swern (18) found a band at 970 cm.$^{-1}$, caused by the formation of *trans* isomers during autoxidation of methyl oleate, and related it to peroxide formation. In this work, absorption due to *trans* double bonds continued to increase long after peroxide values had decreased.

TABLE IV

THE EFFECT OF INCUBATION TEMPERATURE AND OF TIME ON ABSORPTION AT 974 CM.$^{-1}$ (*trans* ISOMERS)

Time in weeks	Incubation temperatures			
	40°C.	60°C.	80°C.	100°C.
	$\log \frac{I_0}{I}$			
2	0.03	0.08	0.16	0.25
4	0.09	0.12	0.38	0.40
8	0.16	0.34	0.47	0.59
10	0.21	0.44	0.52	0.67
12	0.32	0.52		
16	0.45	0.66		
20	0.64	0.75		
26	0.85	0.87		
32	1.0	1.02		

The spectra of samples in which autoxidation was advanced had two broad bands with maxima at approximately 821 and 899 cm.$^{-1}$ and also a strong band above 1040 cm.$^{-1}$. The significance of these bands is not known. The increase in free fatty acids in the highly autoxidized samples was probably responsible for a weak band at about 936 cm.$^{-1}$.

The effect of iron on autoxidation was not detectable by infrared absorption in this region of the spectrum.

After incubation for 13 weeks at 100°C. the first band at 988 cm.$^{-1}$ had disappeared but the second peak at 974 cm.$^{-1}$ was strong. The 13 week samples with and without added iron were distilled and it was found that almost all of the component causing absorption at 974 cm.$^{-1}$ was in the residues. Both residues and distillates gave rise to broad weak peaks at 821 and 899 cm.$^{-1}$ as well as a region of strong absorption above 1040 cm.$^{-1}$. Absorption by the distillate from the esters with added iron was considerably weaker than by the distillate obtained from the autoxidized esters. Absorption by the residue from the esters containing added iron was stronger than that from the control esters in this region.

When the sample of esters, incubated at 100°C. for 13 weeks was divided into four fractions by means of the Craig extraction apparatus, there was no real separation of absorption bands. The four fractions had spectral curves with the same characteristics as the unextracted, autoxidized sample, Fraction 1 being identical to it. Spectral curves of Fraction 2, 3, and 4 were found to be similar but of increasing intensities. Fraction 4 had intense absorption below 1040 cm.$^{-1}$.

Conclusions

The infrared spectrometer can be used to measure the development of hydroxyl and carbonyl groups, and the formation of *trans* isomers and of conjugated unsaturation during autoxidation of unsaturated fatty acid esters. This instrument should prove to be useful in the study of the mechanism of autoxidation, particularly when the products of autoxidation have been more completely fractionated and when the absorption spectra of model compounds have been determined.

Acknowledgment

The authors wish to acknowledge the able technical assistance of Mr. V. R. Thomson.

References

1. Allen, R. R., Jackson, A., and Kummerow, F. A. J. Am. Oil Chemists' Soc. 26: 395-399. 1949.
2. American Oil Chemists' Society. Official and tentative methods. 2nd ed. A.O.C.S., Chicago, 1946.
3. Bergstrom, S. and Holman, R. T. Nature, 161: 55. 1948.
4. Better, E. J., and Davidsohn, A. Oil and Soap, 23: 283-284. 1946.
5. Bolland, J. L. and Koch, H. P. J. Chem. Soc. 445-447. 1945.
6. Cole, J. O. and Field, J. E. Ind. Eng. Chem. 39: 174-179. 1947.
7. Craig, L. C. and Post, O. Anal. Chem. 21: 500-504. 1949.
8. Dugan, L. R., Beadle, B. W., and Henick, A. S. J. Am. Oil Chemists' Soc. 26: 681-685. 1949.
9. Farmer, E. H. Trans. Faraday Soc. 42: 228-236. 1946.
10. Farmer, E. H., Bloomfield, G. F., Sundralingham, A., and Sutton, D. A. Trans. Faraday Soc. 38: 348-356. 1942.
11. Farmer, E. H., Koch, H. P., and Sutton, D. A. J. Chem. Soc. 541-547. 1943.
12. Graff, M. M., O'Connor, R. T., and Skau, E. L. Ind. Eng. Chem., Anal. Ed. 16: 556-557. 1944.
13. Gunstone, F. D. and Hilditch, T. P. J. Chem. Soc. 836-841. 1945.
14. Henick, A. S. Food Technol. 5: 145-147. 1951.
15. Hickman, K. C. D. and Sanford, C. R. J. Phys. Chem. 34: 637-653. 1930.
16. Honn, F. J., Bezman, I. I., and Daubert, B. F. J. Am. Chem. Soc. 71: 812-816. 1949.
17. Hess, P. S. and O'Hare, G. A. Ind. Eng. Chem. 42: 1424-1431. 1950.
18. Knight, H. B., Eddy, C. R. and Swern, D. J. Am. Oil Chemists' Soc. 28: 188-192. 1951.
19. Lemon, H. W., Knapp, Ruth M., and Allman, A. H. Can. J. Research, F, 28: 453-460. 1950.
20. Loury, M. and Mellier, M. T. Oléagineux, 4: 665-668. 1949.
21. Lundberg, W. O. Oléagineux, 4: 86-94. 1949.
22. Lundberg, W. O. and Chipault, J. R. J. Am. Chem. Soc. 69: 833-836. 1947.
23. Mattill, H. A. Oil and Soap, 18: 73-76. 1941.
24. Paschke, R. F., and Wheeler, D. H. Oil and Soap, 21: 52-57. 1944.
25. Powers, P. O. Ind. Eng. Chem. 41: 304-309. 1949.
26. Shreve, O. D., Heether, M. L., Knight, H. B., and Swern, D. Anal. Chem. 23: 282-285. 1951.
27. Sims, R. P. A. Can. Chem. Process Inds. 35: 125-129, 133. 1951.
28. Skellon, J. H. and Thruston, M. L. J. Chem. Soc. 1626-1630. 1949.
29. Swern, D., Scanlan, J. T., and Knight, H. B. J. Am. Oil Chemists' Soc. 25: 193-200. 1948.
30. Wheeler, D. H. Oil and Soap, 9: 89-97. 1932.

NOISE SUPPRESSION IN TRIODE AMPLIFIERS. II[1]

By A. van der Ziel[2]

Abstract

Experiments on triode amplifier stages at 10 m. wave length are reported, which were carried out in order to test the theory presented in a previous paper (to be called I). The theory of the noise factor of triode stages is first put into a form which allows experimental verification. In paper I it was shown that a capacitive feedback between input and output of a grounded cathode amplifier stage might improve the noise factor considerably. A comparison between a grounded cathode circuit with tuned anode–grid capacity C_{ag} and the same circuit with untuned anode–grid capacity (obtained by removal of the tuning coil) shows that the latter is only slightly better than the former one and that the small improvement is mainly due to the removal of the coil tuning the anode–grid capacity. Moreover, the circuit has the tendency to oscillate at a frequency differing slightly from the tuning frequency. It is also shown that some improvement in the noise factor of a grounded cathode circuit with tuned C_{ag} can be obtained by properly detuning the input circuit. The improvement is limited by the thermal noise of the input circuit and by the uncorrelated part of the induced grid noise. Measurements of the correlated and uncorrelated part of the induced grid noise are presented and it is shown that for 6J4 and 6AC7 tubes only 30–40% of the induced grid noise is correlated to the tube noise itself. It is finally shown that the noise factor of a grounded grid circuit and of a grounded cathode circuit with tuned anode–grid capacity and properly detuned input circuit are identical as required by the theory.

Introduction

In a previous paper (5) of the same title (which will be called I) a feedback triode circuit was discussed which theoretically should give a noise factor close to unity, much better than the noise factor of more conventional circuits. It is the aim of this paper to show the extent to which this ideal can be realized in practice.

The circuit consisted of a grounded cathode circuit with untuned anode–grid capacity C_{ag} in which an additional feedback capacity might be inserted in parallel to C_{ag}.

The possible improvement was found to depend largely upon the following factors:

(1) The influence of the thermal noise of the input circuit,

(2) The stability of the circuit,

(3) The possibility that part of the induced grid noise is *not* correlated to tube noise.

It is the aim of this paper to analyze these factors experimentally.

[1] *Manuscript received August 6, 1951.*
Contribution from the Department of Physics, The University of British Columbia, Vancouver, B.C.

[2] *Present address: Department of Electrical Engineering, University of Minnesota, Minneapolis, Minn.*

In our measurements we used a linear amplifier of which the stage under investigation formed the first stage. We used two noise diodes, one across the input circuit of the stage and one across the output circuit of the stage. The latter is needed in order to correct for any change in internal impedance of the stage in a manner presented in a previous paper (4). The noise output power was measured with a quadratic detector (crystal diode) and the detected current was measured with a galvanometer. The detected current was found to be directly proportional to the noise output power of the amplifier. The tuning condenser of the input circuit was calibrated so that the noise factor and all other quantities of interest could be measured as a function of the tuning capacity C.

Theory

In order to give a theoretical interpretation of these measurements, the theory has to be presented in a slightly different manner than that in I. The two theories are equivalent, the only advantage of the new theoretical approach is that it is more convenient for the discussion of the present measurements. We have to consider two cases: (*a*) detuned input circuit, tuned anode–grid capacity, (*b*) detuned input circuit, untuned anode–grid capacity.

Consider a grounded cathode circuit using a triode. Let i_1 be the noise current flowing *to* the anode, and let i_0 be that part of the noise current flowing *from* the cathode that is completely correlated to i_1. Then a noise current $(i_0 - i_1)$ which is completely correlated to i_1 is flowing to the grid. It may be that the noise current flowing from the cathode contains a small component which is *not* correlated to i_1; this component is flowing to the grid and is added quadratically to $(i_0 - i_1)$ in order to produce the total induced grid noise. It may well be, of course, that this uncorrelated component is zero; that has to be decided by experiment. At any rate, i_0/i_1 is a complex nonfluctuating quantity.

Let a voltage V_g be applied to the grid, this gives rise to a current $g_0 V_g$ flowing *from* the cathode and a current $g_1 V_g$ flowing *to* the anode, then a current $(g_0 - g_1)\ V_g$ flows to the grid; $(g_0 - g_1)$ denotes the input admittance of the tube due to transit time effects.

We now introduce the noise resistance R_n by the definition:

$$\overline{i_1^2} = 4k\mathrm{T}R_n\,\Delta f\,|\,g_1\,|^2\,. \tag{1}$$

Let an admittance Y_g be connected between grid and ground, and a feedback admittance Y between grid and anode. As usual, we assume in our theoretical discussion that the output is short-circuited. Y_g consists of the transformed antenna resistance R_a, the tuned circuit resistance R_c, and a (positive or negative) capacity C in parallel, C denotes the possible detuning of the input circuit. Hence:

$$Y_g = 1/R_a + 1/R_c + j\omega C. \tag{2}$$

R_a has a noise ratio equal to unity, its noise may be described by a noise current i_a flowing into the input circuit. R_c itself gives thermal noise which

can be described by a noise current i_c flowing into the input. But, in order to take into account that uncorrelated part of the induced grid noise, we incorporate this noise into i_c. Hence:

$$\overline{i_a^2} = 4kT\,\Delta f/R_a;\ \ \overline{i_c^2} = \alpha \cdot 4kT\,\Delta f/R_e\,. \tag{3}$$

If this uncorrelated part does not exist, we have $\alpha = 1$. The actual value has to be decided by experiment.

We should, perhaps, also take into account that the self-induction of the cathode lead gives an additional input damping. But, as this affects signal and noise in the same ratio, we can as well omit it in our discussion.

Y is either practically equal to zero if C_{ag} is tuned or equal to $j\omega C_{ag}$ (the admittance due to the anode–grid capacity) if C_{ag} is untuned. If we put:

$$Y = j\omega C_{ag};\ Y_e = g_0 - g_1 = 1/R_e + j\omega C_e \tag{4}$$

(C_e is the change in input capacity due to space charge effects, R_e is the input resistance due to transit time effects), we have for the input impedance of the circuit for a short-circuited output in the latter case:

$$Y_g + Y + g_0 - g_1 = (1/R_a + 1/R_e + 1/R_c) + j\omega(C + C_e + C_{ag})\,. \tag{5}$$

In the case of tuned anode–grid capacity, we put $C_{ag} = 0$ and incorporate the tuned circuit impedance of the grid–anode circuit in R_c. This means that the value of R_c will differ in the two cases.

As output current = input current × input impedance × transconductance, we can calculate the contribution of antenna noise, circuit noise, and tube noise to the mean square value of the total noise current in the output lead as follows (Fig. 1):

i_a gives a contribution:

$$4kT\,\Delta f/R_a \cdot \left| Y_g + Y + g_0 - g_1 \right|^{-2} \cdot \left| g_1 - Y \right|^2 \tag{6}$$

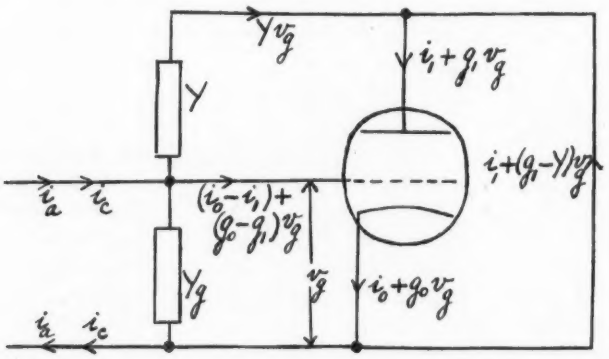

FIG. 1. *Equivalent circuit of a grounded cathode stage with a feedback admittance Y between input and output. The output circuit is short-circuited in order to simplify calculations. The meaning of the various symbols is explained in the text.*

i_c gives a contribution:

$$\alpha \cdot 4kT\,\Delta f/R_c \cdot \left| Y_g + Y + g_0 - g_1 \right|^{-2} \cdot \left| g_1 - Y \right|^2 . \qquad (7)$$

The contribution of tube noise is calculated as follows. The current $(i_0 - i_1)$ flowing through the input gives rise to a voltage:

$$v_g = -(i_0 - i_1)\,(Y_g + Y + g_0 - g_1)^{-1}$$

between grid and cathode and hence to a current:

$$i_1 - (i_0 - i_1)\,(g_1 - Y)\,(Y_g + Y + g_0 - g_1)^{-1} = i_1\,[(Y_g + g_0) - (g_1 - Y)\,i_0/i_1] \cdot (Y_g + Y + g_0 - g_1)^{-1}$$

flowing through the output lead. Hence its contribution is:

$$4kTR_n\,\Delta f \left| g_1 \right|^2 \cdot \left| (Y_g + g_0) - (g_1 - Y)\,i_0/i_1 \right|^2 \cdot \left| Y_g + Y + g_0 - g_1 \right|^{-2}. \qquad (8)$$

The noise factor F is obtained by adding (6), (7), and (8), and dividing by (6):

$$F = 1 + \alpha\,R_a/R_c + R_n\,R_a \left| Y_g + g_0 - g_1\,i_0/i_1 + Yi_0/i_1 \right|^2 \cdot \left| g_1/(g_1 - Y) \right|^2. \qquad (9)$$

We now put $Y = 0$ in case (a), and $Y = j\omega C_{ag}$ in case (b). In both cases, we have that at 10 m. $\left| g_1/(g_1 - Y) \right| = 1$ in very good approximation, so that the corresponding term in (9) can be neglected.

We first discuss case (a). Introducing quantities R_z and C_z by the definition:

$$Y_z = g_0 - g_1\,i_0/i_1 = 1/R_z + j\omega C_z\,; \qquad (10)$$

(9) then becomes:

$$F = 1 + \alpha.\quad R_a/R_c + R_nR_a\,[(1/R_a + 1/R_c + 1/R_z)^2 + \omega^2\,(C + C_z)^2]\,. \qquad (11)$$

This has a minimum value if $C = -C_z$, in which case:

$$F = F_{min} = 1 + \alpha.\quad R_a/R_c + R_n\,R_a\,(1/R_a + 1/R_c + 1/R_z)^2. \qquad (11a)$$

If $\Delta C = (C + C_z) \neq 0$, we have:

$$F = F_{min} + \omega^2\,R_n\,R_a\,(\Delta C)^2. \qquad (11b)$$

As the input circuit is tuned if $C = -C_e$ (compare (5)), we have in that case:

$$F = F_{tuned} = F_{min} + \omega^2\,R_n\,R_a\,(C_e - C_z)^2\,. \qquad (11c)$$

The validity of these formulae can be verified by experiment, the improvement in noise factor by proper detuning can be determined and the values of C_e and C_z can be determined, too.

We turn now to case (b). Introduce quantities C_f and R_f by the definition:

$$Y_f = Yi_0/i_1 = j\omega C_{ag}.\quad i_0/i_1 = -1/R_f + j\omega C_f \qquad (12)$$

(the real part is negative because i_1 is delayed in phase with respect to i_0; as $\left| i_0/i_1 \right|$ is about equal to unity, $C_f = C_{ag}$).

The noise factor now becomes:

$$F = 1 + \alpha.\quad R_a/R_c + R_n\,R_a \left| (1/R_a + 1/R_c + 1/R_z - 1/R_f)^2 + \omega^2\,(C + C_z + C_f)^2 \right|. \qquad (13)$$

This is a minimum if $(C + C_z + C_f) = 0$:

$$F = F^1_{min} = 1 + \alpha. \quad R_a/R_c + R_n R_a (1/R_a + 1/R_c + 1/R_z - 1/R_f)^2 \quad (13a)$$

which is smaller than (11*a*) owing to the term $- 1/R_f$.

Putting $(C + C_z + C_f) = \Delta C^1$, we have in general:

$$F = F^1_{min} + \omega^2 R_n R_a (\Delta C^1)^2 . \quad (13b)$$

We note that (13*b*) and (11*b*) have the same general shape and that the coefficients in front of $(\Delta C)^2$ and $(\Delta C^1)^2$ are identical. This is open to experimental verification.

As we have every reason to believe that R_z is quite large, we may in first approximation neglect R_z in the above formulae.

Instead of the noise factor F we can also introduce the equivalent input saturated diode current I of the stage with the help of the relation:

$$F = (e/2kT)\ IR_a = 20\ IR_a \quad (14)$$

and (11*b*) may be written:

$$I = I_{min} + (2kT/e)\ \omega^2 R_n (C + C_z)^2 \quad (15)$$

so that I should show a minimum value at $C = - C_z$. The meaning of I is that a saturated diode connected across the input carrying a d-c. current I produces as much input noise power as the whole stage. The advantage of introducing the quantity I is that it also exists if $R_a = \infty$ whereas $F = \infty$ in that case. Putting $R_a = \alpha$, we obtain in (15) for $C = - C_z$:

$$I_{min} = (2kT/e)\ [\alpha/R_c + R_n (1/R_c + 1/R_z)^2] . \quad (16)$$

As R_z and R_c are usually very large the last term in (16) can be neglected and we obtain:

$$I_{min} = I'_d = (2kT/e)\ \alpha/R_c . \quad (16a)$$

The meaning of I'_d is that it is the equivalent saturated diode current of the thermal noise of the input circuit + the uncorrelated part of the induced grid noise (if any).

We now tune the input circuit, that is we put $C = - C_e$. In that case:

$$I = I_d = I_{min} + (2kT/e)\ \omega^2 R_n (C_e - C_z)^2 . \quad (17)$$

In order to understand the meaning of the second term we observe that $j\omega C_e$ is the imaginary part of $(g_0 - g_1)$ and $j\omega C_z$ the imaginary part of $(g_0 - g_1\, i_0/i_1)$; consequently $j\omega(C_e - C_z)$ is the imaginary part of $g_1\ (i_0/i_1 - 1)$. But as $\left| i_0/i_1 \right| \approx 1$ in very good approximation at 10 m. wave length, as i_1 is only slightly delayed in phase with respect to i_0 and as g_1 only has a very small phase angle, it may be assumed that $(i_0/i_1 - 1)$ hardly has any real part, so that in good approximation:

$$g_1(i_0/i_1 - 1) = j\omega(C_e - C_z) . \quad (18)$$

Taking the modulus of the square of both sides, and substituting the value for $\overline{i^2}$ from (1) we have:

$$\overline{(i_0 - i_1)^2} = 4kTR_n \, \Delta f \, \omega^2 \, (C_e - C_z)^2 = 2e \, I''_d \, \Delta f \tag{19}$$

so that the correlated part of the induced grid noise is equivalent to an input saturated diode current I''_d. This shows that the second term in (17) presents the correlated part of the induced grid noise. We thus see that

$$I_d = I'_d + I''_d \tag{19a}$$

is the equivalent saturated diode current of the thermal noise of the input circuit + all induced grid noise. By measuring the equivalent saturated diode current we can determine I'_d and I''_d. If we know the impedance of the tuned input circuit we can calculate its corresponding equivalent saturated diode current and thus express the correlated and uncorrelated parts of the induced grid noise in microamperes saturated diode current.

Introducing (17) we may write (11*c*) as:

$$F = 1 + (e/2kT) \, I_d \, R_a + R_n \, R_a \, (1/R_a + 1/R_c + 1/R_z)^2 . \tag{20}$$

If we adjust the tuning of the input circuit such that F is a minimum ($C = -C_z$), we have by substituting (16*a*) in (11*a*):

$$F = 1 + (e/2kT) \, I'_d \, R_a + R_n \, R_a \, (1/R_a + 1/R_c + 1/R_z)^2 . \tag{20a}$$

Owing to the detuning of the input circuit the power gain is less than in the former case but the noise factor is somewhat smaller.

We can also calculate the noise factor F of a grounded grid circuit. We suppress the actual calculation as it is identical to the calculation for the grounded cathode circuit. The final result is identical with (11). The noise factor is a minimum if $C = -C_z$ and in that case the formula for the noise figure is identical with (20*a*). For that reason it is often said that the grounded cathode and the grounded grid circuit have identical noise factors. It should not be forgotten, however, that even though (20*a*) holds for both circuits if $C = -C_z$, the input circuit is practically tuned for the grounded grid circuit, but it is *detuned* for the grounded cathode circuit (1).

We may write (20) and (20*a*) as follows:

$$F = A + B/R_a + CR_a \tag{21}$$

in which:

$$A = 1 + 2 \, R_n \, (1/R_c + 1/R_z); \; C = R_n . \tag{21a}$$

For a grounded cathode stage with tuned input circuit ($C = -C_e$):

$$B = (e/2kT) \, I_d + R_n \, (1/R_c + 1/R_z)^2, \tag{21b}$$

whereas:

$$B = (e/2kT) \, I'_d + R_n \, (1/R_c + 1/R_z)^2 \tag{21c}$$

for the case of minimum noise figure ($C = -C_z$) in both the grounded cathode and the grounded grid circuit. Usually the second term in (21*b*) and (21*c*) is negligible and as $(e/2kT) = 20$ in practical units:

$$B = 20\ I_d, \qquad B = 20\ I'_d, \tag{21d}$$

respectively, in good approximation.

Noise Cancellation in 6J4 Triodes; Stability of the Circuit

In order to demonstrate the pitfalls which have to be avoided here we first discuss some measurements which at first seemed to indicate that an important noise reduction in 6J4 triodes occurred if the coil which tuned the anode–grid capacity was removed. At the same time we answer the question of the stability of the circuit.

In these experiments we measured the noise output power of a receiver as a function of the tuning capacity C of the input circuit of the first stage, consisting of a 6J4 triode in grounded cathode connection with the anode–grid capacity untuned (2). The transformed antenna resistance was 10,000 ohms, the output circuit of the stage was heavily damped by a resistance of 80 ohms in order to avoid oscillations. Though this is only a small resistance, the stage still had a considerable power gain as the input impedance of the stage was estimated to be of the order of 10,000 ohms. The "signal" output power was also measured as a function of the capacity C; this "signal" was simulated by generating a large input noise current with the help of the noise diode (the receiver gain had to be adjusted such that the rectified currents were comparable in the two cases). In both cases the noise background due to the resistance of 80 ohms + the subsequent stages of the receiver was determined by biasing the tube beyond cutoff; the noise background for the "noise" curve is much larger than for the "signal" curve (Fig. 2).

The results are shown in Fig. 2. Instead of deriving the noise factor F from Fig. 2, it is more convenient to use the closely related noise-to-signal ratio.* This ratio may be directly calculated from Fig. 2 as $\dfrac{\text{noise-background}}{\text{signal-background}}$ (note that "noise" and "signal" have different backgrounds). If this ratio is plotted against C it shows a distinct minimum at $C = 55$ divisions. From a measurement of the noise factor for the tuned input circuit ($C = 70$ divisions) it could be estimated that the noise factor at $C = 55$ divisions was very close to unity. This looked rather promising, even though the power gain at that point was not very large.

Unfortunately this promising result was erroneous. For in Fig. 2 the background curves were drawn as straight lines, because it might be thought that the load resistance of 80 ohms would be very small in comparison with the

* *Defined as the ratio:* $\dfrac{\textit{noise output power due to the first stage only}}{\textit{signal output power}} = \dfrac{F.\,kTB}{\textit{available signal power at input}}$, *where B is the band width of the noise amplifier.*

output resistance of the stage. But owing to feedback through the capacity C_{ag} the output conductance varies between a large positive and a large negative value. It was actually found with the help of the output noise diode of the stage (2) that the output circuit was heavily damped around $C = 55$ divisions. The background curve belonging to the "noise" curve should show a dip around $C = 55$ divisions and the actual noise figure at that point should be much larger than was first anticipated (under certain conditions it would have been possible to find noise factors less than unity in this way). By taking due account of the influence of the output impedance of the stage upon the background noise we actually found that the noise factor was not much better than with tuned anode–grid capacity (see below).

An analysis of the circuit showed that the circuit was perfectly stable at the normal point of operation but that it had a tendency to oscillate at a slightly different frequency unless the output circuit of the stage was heavily damped.

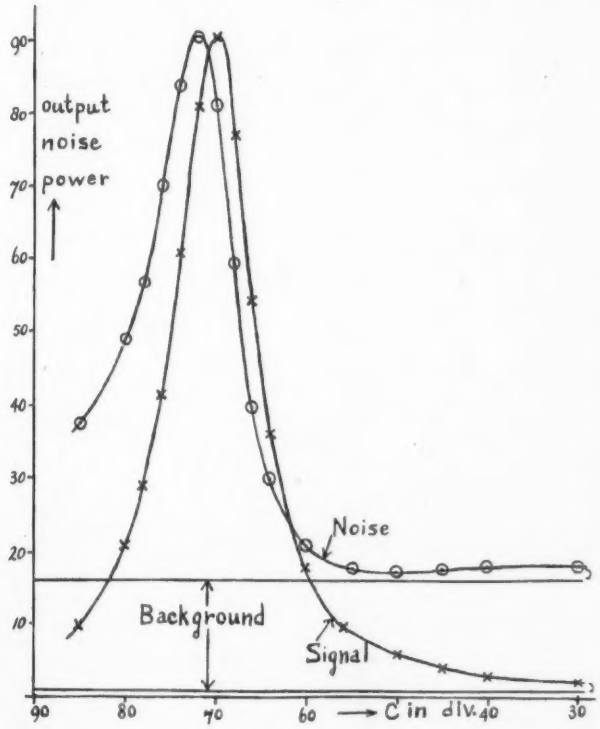

FIG. 2. *Noise output power and signal output power of a receiver as a function of the tuning capacity C of the input circuit of the receiver on an arbitrary scale. The first stage of the receiver is a grounded cathode stage with untuned anode–grid capacity. The noise background due to the remaining part of the receiver in both cases was determined by biasing the first tube of the receiver beyond cutoff. The "signal to noise ratio" appears to be largest for $C = 55$ divisions. It is explained in the text how one may draw quite erroneous conclusions from these types of curves (note that increasing number of divisions corresponds to decreasing capacity).*

Noise Factor F as a Function of R_a for 6J4 Tubes for the Case of Tuned Anode–Grid capacity and Tuned Input Circuit at 10 m. Wave Length (3)

We measured several 6J4 tubes but give the measurements on tube No. 2 in more detail as this tube was much used in the other experiments. Table I

TABLE I

NOISE FACTOR F OF 6J4 TUBE NO. 2; $V_a = 150$ v.; $I_a = 10$ ma.

R_a in ohms	$F_{obs.}$	$F_{calc.}$
9800	2.98	2.99
5100	2.10	2.12
2400	1.79	1.68
1000	1.56	1.57
600	1.70	1.68
350	1.95	1.97
204	2.51	2.51

gives the results. The calculated values were obtained from a formula of the type (21); the constants A, B, and C were chosen such that the closest fit was obtained with the observed data. We see that the calculated values for F fit closely with the experimental ones.

In Table II we give the values for A, B, and C for four 6J4 tubes including the tube of Table I.

TABLE II

COEFFICIENTS A, B, AND C FOR 6J4 TUBES

Tube Number	A	$B \times 10^4$	I_d (μa.)	Total induced grid noise (μa.)	$C = R_n$ (ohms)
1	1.10	1.30	6.5	2.3	320
2	1.10	1.90	9.5	5.3	280
4	1.10	1.45	7.3	3.1	330
5	1.10	1.75	8.7	4.5	330

We also calculated the equivalent saturated diode current I_d of circuit noise + induced grid noise from the formula for B. We measured from the resonance curve, with the tube biased beyond cutoff, for R_c a value of 12,000 ohms. This corresponds to an equivalent saturated diode current of 4.2 μa. Subtracting this from I_d we obtain the total induced grid noise in μa. equivalent saturated diode current. The various tubes show a rather large spread.

Taking $R_c = 12{,}000$ ohms and $R_n = 300$ ohms and assuming R_z to be very large, we obtain $A = 1.05 - 1.06$ which is slightly smaller than the measured value of 1.10.†

† *The accuracy of the measurements does not warrant the drawing of very definite conclusions about R_z, except that R_z is probably large.*

Comparison of the Cases of Tuned and Untuned Anode–Grid Capacity for 6J4 Tubes at 10 m. Wave Length

In this section we compare measurements on 6J4 stages at 10 m. wave length for the case of tuned and untuned anode–grid capacity C_{ag}. In each case we compare the experimental results with the theoretical formulae (11*b*) and (13*b*) and determine equations of the type (11*b*) or (13*b*) which give the closest fit to the experimental data. The results are shown in Table III. We see that the observed and calculated values agree very well.

TABLE III

NOISE FACTOR OF 6J4 TUBE No. 2; $V_a = 150$ v.; $I_a = 10$ ma.

Cap. in divisions	C_{ag} tuned				Cap. in divisions	C_{ag} untuned	
	$R_a = 9800$ ohms		$R_a = 2400$ ohms			$R_a = 2400$ ohms	
	Obs.	Calc.	Obs.	Calc.		Obs.	Calc.
65	5.88	5.85	2.11	2.12	80	2.12	2.12
60	4.51	4.36	1.81	1.81	75	1.83	1.80
55	3.27	3.33	1.61	1.61	70	1.62	1.56
50	2.74	2.74	1.52	1.52	65	1.48	1.49
45	2.61	2.61	1.53	1.53	60	1.51	1.51
40	2.94	2.93	1.67	1.67	55	1.71	1.62
35	3.72	3.69	1.86	1.86	50	1.86	1.85
30	4.68	4.90	2.18	2.19	45	2.15	2.19

The calculated values were obtained with the help of the following formulae:

(*a*) C_{ag} tuned, $R_a = 9800$ ohms:

$$F = 2.60 + 0.90 \times 10^{-2}(C - 46.0)^2 = 2.60 + 0.106(\Delta C)^2. \quad (22a)$$

(*b*) C_{ag} tuned, $R_a = 2400$ ohms:

$$F = 1.51 + 0.21 \times 10^{-2}(C - 48.0)^2 = 1.51 + 2.50 \times 10^{-2}(\Delta C)^2. \quad (22b)$$

(*c*) C_{ag} untuned; $R_a = 2400$ ohms:

$$F = 1.48 + 0.22 \times 10^{-2}(C - 63.0)^2 = 1.48 + 2.60 \times 10^{-2}(\Delta C)^2. \quad (22c)$$

Another set of measurements gave:

$$F = 1.43 + 0.20 \times 10^{-2}(C - 63.0)^2 \quad (22d)$$

showing the consistency of the measurements. The accuracy for case (*c*) was somewhat smaller than for the other cases because the noise output had to be corrected for the change in output impedance of the stage (2).

In the first set of equations the capacities are expressed in divisions, in the second set of equations ΔC is expressed in $\mu\mu$f.; the conversion is obtained by observing that 1 division corresponds to 0.29 $\mu\mu$f. We observe that the coefficients in front of ΔC for the cases (*b*) and (*c*) are equal within the limits of

accuracy as required by the theory. From the value of the coefficients in the cases (*a*) and (*b*) we can deduce with the help of (11*b*) and (13*b*):

$$R_n = 305 \text{ ohms in case } (a),\ R_n = 295 \text{ ohms in case } (b).$$

The mutual agreement is very good and so is the agreement with the value $R_n = 280$ ohms found in the previous section for the same tube.

The values of C_e and C_z were also measured for the cases of tuned anode–grid capacity for $R_a = 9800$ ohms and $R_a = 2400$ ohms. The measurement for $R_a = 9800$ ohms is more accurate than the latter one as the resonance curve of the input circuit was much sharper.

We found for $R_a = 9800$ ohms that the input circuit was tuned at 45.0 divisions if the tube was biased beyond cutoff; at 10 ma. anode current the input circuit was tuned at 51.8 divisions; the increase C_e in input capacity due to space charge was thus found to be 6.8 divisions = 2.0 $\mu\mu$f. F was found to have its minimum at 46 divisions hence $C_z = 1.0$ divisions = 0.3 $\mu\mu$f. Consequently $C_e - C_z = 5.8$ divisions = 1.7 $\mu\mu$f.

The measurements at $R_a = 2400$ ohms, though less accurate, yielded the result that for $I_a = 10$ ma. the input circuit was now tuned at 54.2 divisions whereas F was a minimum at 48 divisions. Consequently $(C_e - C_z) =$ 6.2 divisions = 1.8 $\mu\mu$f., in good agreement with the former value.

Applying formula (19) we see that I''_d, the correlated part of the induced grid noise, amounts to 1.6 μa. As the total induced grid noise I_d amounted to 5.3 μa., we find from (19*a*) that the uncorrelated part of the induced grid noise amounts to 3.7 μa. equivalent saturated diode current, so that only 30% of the induced grid noise is correlated with the tube noise whereas 70% is uncorrelated. We did not measure the same quantities for other 6J4 tubes; some measurements on 6AC7 tubes connected as triodes are reported in the next section.

We are now able to compare the results for 6J4 tube No. 2 with $R_a =$ 2400 ohms under the following conditions.

(*a*) Input circuit tuned; anode–grid capacity tuned: $F = 1.60$.
(*b*) Input circuit properly detuned; anode–grid capacity tuned: $F = 1.51$.
(*c*) Input circuit properly detuned; anode–grid capacity detuned $F = 1.46$.

The result quoted under (*a*) is derived from (22*b*) by putting $C = 54.2$ divisions, the result under (*b*) is obtained from (22*b*) ($\Delta C = 0$), the result under (*c*) from (22*c*) and (22*d*) ($\Delta C = 0$).

We see that the difference between the cases (*b*) and (*c*) is only small. We can understand this as follows: From (18) we have:

$$\frac{i_0}{i_1} = 1 + j\omega(C_e - C_z)/g_1\,, \tag{23}$$

so that $1/R_f$, which is defined as the real part of Y_f (Equation (12)):

$$1/R_f = -\omega^2\, C_{ag}(C_e - C_z)/g_1\,. \tag{23a}$$

Putting $C_{ag} = 4.4$ $\mu\mu$f., $(C_c - C_z) = 1.7$ $\mu\mu$f. (both measured) and estimating $g_1 = 10^{-2}$ mhos gives $R_f = -38{,}000$ ohms. This value is so large that it can hardly have any effect upon F. The main difference in F is due to the removal of the tuning coil of the anode–grid capacity. Owing to the finite Q of the coil, the measured value of the tuned circuit impedance was 60,000 ohms; removal of this impedance caused a decrease in I'_d by 0.8 μa. Inserting this into (16*a*) and (11*a*) we obtain a reduction of 0.04 in F. Though this difference is within the limit of error it happens to agree with the measured difference of 0.05. We conclude:

It is not worthwhile to use a stage with untuned anode–grid capacity. If C_{ag} is tuned, it is *worthwhile, however, to detune the input circuit properly, though the decrease in F is not spectacular.*

With C_{ag} untuned and $R_a = 2400$ ohms the input circuit was tuned at $C = 80$ divisions and $F = 2.12$ at that point; with C_{ag} tuned and $R_a = 2400$ ohms the input circuit was tuned at $C = 54.2$ divisions and $F = 1.60$ (Table II) at that point. This is perhaps the reason why it is sometimes thought that the noise factor becomes worse when C_{ag} is not tuned (3). The above measurements indicate that this is not true; if the input circuit is properly detuned, F can be at least as good as for tuned anode–grid capacity.

Correlated Part of the Induced Grid Noise in 6AC7 Tubes

We measured the equivalent input saturated diode current I of a stage using 6AC7 tubes connected as triodes. We obtained the results shown in Table IV. The measurements are well represented for the formulae,

$$\text{Tube No. 1.} \quad I = 14.9 + 0.095\,(C - 61.3)^2\ \mu\text{a.} \tag{24a}$$

$$\text{Tube No. 2.} \quad I = 10.1 + 0.080\,(C - 59.5)^2\ \mu\text{a.} \tag{24b}$$

from which the "calculated" values of Table IV were calculated. From (15), (24*a*), and (24*b*) we obtain $R_n = 640$ ohms for Tube No. 1 and $R_n = 540$ ohms

TABLE IV

6AC7. I IN μa. FOR TUBES NOS. 1 AND 2. $V_a = V_{g2} = 150$ v.; $(I_a + I_{g2}) = 10$ ma.

Cap. in divisions	Tube No. 1		Tube No. 2	
	Obs.	Calc.	Obs.	Calc.
47.5	—	—	21.9	21.7
50.0	28.3	27.1	17.4	17.3
52.5	21.4	22.3	13.5	14.0
55.0	18.6	18.7	12.0	11.7
57.5	15.8	16.3	10.4	10.4
60.0	15.1	15.1	9.5	10.1
62.5	15.1	15.0	10.5	10.8
65.0	15.4	16.2	12.1	12.3
67.5	18.5	18.6	15.1	15.2
70.0	23.1	22.1	20.0	18.9
72.5	—	—	23.5	23.7

for Tube No. 2; this fits rather well with the values of 600 ohms and 500 ohms obtained by other methods.

It was found by passing a large saturated current through the input noise diode that the signal was a maximum at 68.1 divisions for Tube No. 1 and at 65.7 divisions for Tube No. 2. This shows that

$$(C_e - C_z) = 6.8 \text{ divisions for Tube No. 1,}$$
$$(C_e - C_z) = 6.2 \text{ divisions for Tube No. 2.}$$

Introducing this into (19) we obtain:

$$I''_d = 4.4 \ \mu\text{a. for Tube No. 1;} \quad I''_d = 3.1 \ \mu\text{a. for Tube No. 2.}$$

We also measured the input circuit impedance R_e in the case of zero tube current and found a value of 9400 ohms, corresponding to an equivalent saturated diode current of 5.3 μa. Subtracting this value from I_{min} we obtain the following results:

Tube No. 1. Induced grid noise 14.0 μa., correlated part 4.4 μa., uncorrelated part 9.6 μa.

Tube No. 2. Induced grid noise 7.9 μa., correlated part 3.1 μa., uncorrelated part 4.8 μa.

This shows again a large spread in values for different tubes, but also that *a large part of the induced grid noise is not correlated to tube noise.*

Measurements on 6J4 Tubes in a Grounded Grid Stage

We also carried out measurements on some 6J4 tubes in a grounded grid circuit. The measurements are by no means as accurate as for the grounded cathode circuit, especially for large values of R_a; this is due to the fact that the gain of the stage is so small in that case. The measurements on 6J4 Tube No. 2 could be represented by the formula

$$F = 1.08 + 280/R_a + 1.70 \times 10^{-4} R_a$$

so that $R_n = 280$ ohms, in perfect agreement with the value from Table II. From the coefficient 1.70×10^{-4} we deduce that $I'_d = 8.5$ μa. From the measurements in Section 5 we found $I_d = 9.5$ μa.; $I''_d = 1.6$ μa. and thus $I'_d = 7.9$ μa. In view of the inaccuracy of the measurement this is a perfect agreement.*

We may conclude from the above experiments that the noise figure of a grounded grid stage is practically equal to the noise figure of a grounded cathode stage with tuned anode–grid capacity and properly detuned input circuit as required by the theory.

* *The agreement is not as good as it looks at first sight. We measured $R_e = 8300$ ohms for our grounded grid stage, corresponding to 6.0 μa. saturated diode current, so that the uncorrelated part of the induced grid noise is 2.5 μa. This has to be compared with the value of 3.7 μa. measured in Section 5. This is still well within the limit of accuracy, however.*

Conclusions

(*a*) The stage with untuned anode–grid capacity and properly detuned input circuit is stable in its operating point but it shows the tendency to oscillate at a slightly different frequency unless the output circuit is heavily damped.

(*b*) If the input circuit is tuned, then the noise factor for untuned C_{ag} is *much larger* than for tuned C_{ag}.

(*c*) If the input circuit is properly detuned then the noise factor for untuned C_{ag} is slightly smaller than for tuned C_{ag}; the difference is so small that it is certainly not warranted to operate the tube in that complicated way.

(*d*) Some improvement in noise figure can be obtained by properly detuning the input circuit for the case of tuned C_{ag}. The improvement is not very spectacular either, mainly because a large part of the induced grid noise is not correlated to tube noise.

(*e*) The grounded grid circuit and the grounded cathode circuit have practically identical noise figures as required by the theory (1).

(*f*) The main obstacles for an improvement in noise figure are the thermal noise of the input circuit and the uncorrelated part of the induced grid noise. It is certainly possible to increase R_c far above the used value of 12,000 ohms, but finally the improvement is limited by the uncorrelated part of the induced grid noise. Some further study on the nature of this uncorrelated part would be worthwhile.

Acknowledgment

This work was carried out under contract with the Defence Research Board of Canada. The author would like to thank the Defence Research Board for granting permission to publish these results and Mr. R. B. Tomlinson for building the equipment.

References

1. KLEEN, W. Frequenz, 3: 209-216. 1949.
2. KNOL, K. S. and VERSNEL, A. Physica, 15: 462-464. 1949.
3. WALLMAN, H., MACNEE, A. B., and GADSDEN, C. P. Proc. Inst. Radio Engrs. 36: 700-708. 1948.
4. ZIEL, A. VAN DER. Philips Research Repts. 2: 321-330. 1947.
5. ZIEL, A. VAN DER. Can. J. Research, F, 28: 189-198. 1950.

CONTENTS OF VOLUME 29

ADAMS, G. A.—Separation of starch and gluten. VI. Starch recovery and purification, 217.
ALLAN, A. B.—See King, R. O.
BAKER, B. E.—See Hare, J. H.
BARBER, V. T.—See Cullen, A. M.
BARNES, W. H. and WAGNER, S.—An X-ray diffraction Laue microcamera, 337.
BARNWELL, J. L.—See Murphy, D.
BLACKWOOD, A. C.—See Neish, A. C.
BOULET, M. and PEARCE, J. A.—Dried whole egg powder. XXIX. The effect of high moisture content on fluorescence and other chemical changes, 153.
BOURNE, B. E.—See McKinley, D. W. R.
BOURNS, A. N.—See Evans, T. H.
BRABANT-SMITH, A. M. K.—Color in margarine. I. Evaluation of color using the Lovibond tintometer, 290. II. An indirect method for measurement of color in terms of the Lovibond color system, 296. III. Effect of storage conditions, 303.
BRADFIELD, R. D.—See Bucher, G. E.
BRAID, P. E. and KAY, K.—A field method for the determination of halogenated hydrocarbons, 159.
BUCHER, G. E. and BRADFIELD, R. D.—A syringe-head for attachment of glass capillary needles to glass syringes, 520.
BURR, A. C.—A radial heat flow apparatus for the determination of thermal conductivity, 451.
CAMPBELL, J. A.—See Murray, T. K.
CHAPMAN, R. A.—See Murray, T. K.
CLARK, R. H.—See Phillips, N. E.; Reynolds, W. L.
COHEN, M.—See Sereda, P. J.
CRAIG, B. M.—See Youngs, C. G.
DAVIS, S. G., FORAN, M. R., OGILVIE, J. D. B., PEARCE, J. A., and WINKLER, C. A.—Dynamic adsorption of ammonia, of butane, of cyanogen chloride, and of water vapor by charcoals, 190.
DION, H. G.—See Kristjanson, A. M.
DJINGHEUZIAN, L. E. and WARREN, T. E.—A study of cold-water separation of bitumen from Alberta bituminous sand on a pilot plant scale, 170.
DURAND, E. J.—See King, R. O.
ELLIOTT, F. H.—Determination of the characteristics of a flame photometer and effects of interfering substances, 111.
ERDMAN, I. E. and THORNTON, H. R.—Psychrophilic bacteria in Edmonton milk and cream. I. Numbers, 232. II. Kinds, 238.
EVANS, T. H. and BOURNS, A. N.—Vapor-phase production of dimethylaniline, 1.
FORAN, M. R.—See Davis, S. G.
FORD, E. G.—A rapid polarographic determination of copper, cadmium, and zinc in silver base alloys, 61.
FRY, F. E. J.—A fractionating column to provide water of various dissolved oxygen content, 144.
GIBBONS, N. E., ROSE, D., and HOPKINS, J. W.—Canadian Wiltshire bacon. XXXI. Effects of salt content and storage temperature on storage life, 458.
GRACE, N. H. and ZUCKERMAN, A.—Canadian erucic acid oils. VI. Blowing of rapeseed, mustard seed, and weed seed oils, 71. VII. Preparation of sulphated and hydroxy acids from rapeseed oil acids, 276.
GRANT, G. A., KATZ, M., and HAINES, R. L.—A modified iodine pentoxide method for the determination of carbon monoxide, 43.
GRANT, G. A., KATZ, M., and RIBERDY, R.—The oxidation of carbon monoxide by solid silver permanganate reagents. III. Effect of method of preparation on activity, 511.
HAINES, R. L.—See Grant, G. A.

HARE, J. H. and BAKER, B. E.—The precipitation of whey proteins using waste sulphite liquor, 332.
HARMSEN, G. W.—See Murphy, D.
HAYWARD, A. M.—See Wright, R. H.
HOPKINS, J. W.—See Gibbons, N. E.
JOHNSON, A. L.—See Reynolds, W. L.
KATZ, M.—See Grant, G. A.
KAY, K.—See Braid, P. E.
KING, R. O., DURAND, E. J., and ALLAN, A. B.—The oxidation, decomposition, ignition, and detonation of fuel vapors and gases. XVII. The nuclear ignition of *n*-pentane in the C.F.R. engine and the effect on performance, 52. XVIII. The operation of a carburetor type engine by compression ignition with diethyl ether or acetaldehyde as the fuel, 382.
KIRBY, E. M.—See Lemon, H. W.
KLASSEN, J.—See Plewes, A. C.
KNAPP, R. M.—See Lemon, H. W.
KRISTJANSON, A. M., DION, H. G., and SPINKS, J. W. T.—Hollow cylinder method of measurement of P^{32} in plants, 496.
LANE, D. A.—See Spinks, J. W. T.
LEMON, H. W., KIRBY, E. M., and KNAPP, R. M.—Autoxidation of methyl esters of peanut oil fatty acids, 523.
MCKINLEY, D. W. R. and BOURNE, B. E.—A precision radio time signal system, 428.*
MAHON, J. H.—See Murray, T. K.
MALLARD, T. M.—See Youngs, C. G.
MATHESON, D. H.—Inorganic nitrogen in precipitation and atmospheric sediments, 406.
MUIRHEAD, D. R.—See Murphy, D.
MURPHY, D.—A study on the possible production of glycerol from sulphite waste liquor by yeast, 471.
MURPHY, D. and STRANKS, D. W.—The production of 2,3-butanediol from sulphite waste liquor, 413.
MURPHY, D., STRANKS, D. W., and HARMSEN, G. W.—Production and properties of 2,3-butanediol. XXXV. Phosphate deficiency as a factor in the production of 2,3-butanediol from sugar-beet molasses, 131.
MURPHY, D., WATSON, R. W., MUIRHEAD, D. R., and BARNWELL, J. L.—Fermentation of beet molasses by *Pseudomonas hydrophila*, 375.
MURRAY, T. K., MAHON, J. H., WRIGHT, A., CHAPMAN, R. A., and CAMPBELL, J. A.—A study of Canadian margarine with particular reference to its vitamin A content, 147.
NEIL, D. J.—A sheet specimen scanner for X-ray diffraction, 84.
NEISH, A. C.—See Tink, R. R.
NEISH, A. C. and BLACKWOOD, A. C.—Dissimilation of glucose by yeast at poised hydrogen ion concentrations, 123.
OGILVIE, J. D. B.—See Davis, S. G.
ORR, R. J. and WILLIAMS, H. L.—Study of the copolymerization of butadiene and styrene in emulsion at subfreezing temperatures, 29.
PEARCE, J. A.—See Boulet, M.; Davis, S. G.
PETERSON, R.—See Rose, D.
PETERSON, R. and ROSE, D.—Estimation of glycogen by the use of anthrone, 317.
PFALZNER, P. M.—The specific heat of wheat, 261.
PHILLIPS, N. E. and CLARK, R. H.—The emulsion polymerization of isoprene. III. The measurement of the amount of vinyl groups, 349.
PLEWES, A. C. and KLASSEN, J.—A study of mass transfer rates from the solid to the gas phase, 322.
PUDDINGTON, I. E.—Electromagnetic mercury pumps for circulating gases, 311.
REYNOLDS, W. L., JOHNSON, A. L., and CLARK, R. H.—The emulsion polymerization of isoprene. II, 343.

*See Additions and Corrections, p. 556.

RIBERDY, R.—See Grant, G. A.
ROSE, D.—See Gibbons, N. E.; Peterson, R.
ROSE, D. and Peterson, R.—Depletion of carbohydrate reserves by starvation and exercise, 421.
ROSE, R. C.—Extraction of alginates from Canadian seaweeds, 19.
ROXBURGH, J. M.—See Tink, R. R.
SACKS, W.—Reduction of the vanadium content of residual petroleum fuels by solvent precipitation, 492.
SEREDA, P. J., THOMAS, W. R., and COHEN, M.—An investigation of the corrosion of domestic hot water tanks, 435.
SIDJAK, N.—An interferometer for the thickness measurement of thin transparent film, 362.
SIMPSON, F. J. and STRANKS, D. W.—Production and properties of 2,3-butanediol. XXXIV. Some factors affecting the fermentation of beet molasses by *Bacillus polymyxa*, 87.
SPENCER, E. Y.—See Tink, R. R.
SPINKS, J. W. T.—See Kristjanson, A. M.
SPINKS, J. W. T., LANE, D. A., and TORCHINSKY, B. B.—A new method for moisture determination in soil, 371.
SPOONER, R. C.—The abrasion resistance of sulphuric acid anodic films on aluminium and its alloys, 479.
STONE, J. E.—The briquetting of straw, 98.
STRANKS, D. W.—See Murphy, D.; Simpson, F. J.
TARR, H. L. A.—Microbiological formation of vitamin B_{12}. I. Production in fish press liquid, 391.
THOMAS, W. R.—See Sereda, P. J.
THORNTON, H. R.—See Erdman, I. E.
TINK, R. R. and NEISH, A. C.—Extraction of polyhydroxy compounds from dilute aqueous solutions by cyclic acetal formation. I. An investigation of the scope of the process, 243.
TINK, R. R. and Roxburgh, J. M.—Extraction of polyhydroxy compounds from dilute aqueous solutions by cyclic acetal formation. III. The continuous extraction of glycerol, 269.
TINK, R. R., SPENCER, E. Y., and ROXBURGH, J. M.—Extraction of polyhydroxy compounds from dilute aqueous solutions by cyclic acetal formation. II. The batch extraction of glycerol, 250.
TORCHINSKY, B. B.—See Spinks, J. W. T.
WAGNER, S.—See Barnes, W. H.
WARREN, T. E.—See Djingheuzian, L. E.
WATSON, R. W.—See Murphy, D.
WEBB, E. L. R.—A continuous motion camera for multiple exposure of 35 mm. film, 401.
WILLIAMS, H. L.—See Orr, R. J.
WINKLER, C. A.—See Davis, S. G.
WOOD, E. E.—The determination of fat and sugar in chocolate, 66.
WRIGHT, A.—See Murray, T. K.
WRIGHT, R. H. and HAYWARD, A. M.—Kinetics of the thermal decomposition of wood, 503.
YOUNGS, C. G., MALLARD, T. M., and CRAIG, B. M.—Photoelectric vacuum controller, 447.
VAN DER ZIEL, A.—Noise suppression in triode amplifiers. II. 540.
ZUCKERMAN, A.—See Grace, N. H.

ADDITIONS AND CORRECTIONS

VOLUME 28

Page 455. In Line 30, milliliters should read cubic millimeters.
Pages 456, 457, and 459. In Figs. 1, 2, 3, and 4, ml. should read cu. mm.
Page 457. In Line 9, ml. should read cu. mm.

VOLUME 29

Page 432. In Line 13, 1/20 sec. should read 1/120 sec.